厚生労働科学研究費補助金（萌芽的先端医療技術開発研究事業）
総括研究報告書

「標的ペプチド付加型感温性ナノミセル及び高周波焦点照射による局所DDSの開発」に関する研究

主任研究者　石坂幸人　国立国際医療センター 難治性疾患研究

研究要旨　標的ペプチドを結合させた磁性体ナノ粒子と MRI を用いて、微少病変を画像化が可能になってきた。本年は、ペプチド-磁性体ナノ粒子を用いたMRI解析を継続して行うとともに、近年の抗体医薬の急速な進展を考慮し、これまでのシステムに加えて抗体を用いた MRI 解析のためのシステム構築のための基礎検討を行った。即ち、プロテイン A の抗体結合領域に由来するペプチド（以下 Z33）を磁性体ナノ粒子に結合し、どんな抗体も混和するだけで磁性体ナノプローブが作成できる簡便なシステムの開発を試みた。一方、温度に反応して融解するリポソームについては、温度応答性の改善を行った。

分担研究者
長谷川正勝　名糖産業名古屋研究所長
河野健司　大阪府立大学工学部教授
湯尾　明　国立国際医療センター
血液疾患研究部長
畠　清彦　(財)癌研究会附属病院化学療法部長
山下克美　金沢大学大学院教授

A. 研究目的

本課題は、標的ペプチドを結合させた磁性体ナノ粒子等を用いて、特異的な画像を取得する一方、温度で融解するリポソームと抗癌剤を使用することで、加温誘導による局所 DDS を可能にするためのシステム開発を目的としている。これまでの解析から、ペプチドによる MRI 画像化が可能になってきたが、一方でヒト型抗体を用いた抗体医薬が急速に進展していることを受け，磁性体ナノ粒子に Z33 というペプチドを介して抗体を結合させるための条件検討を行った。Z33 は、抗体に強く結合するプロテイン A と呼ばれる蛋白質の抗体結合ドメインで、Z33-磁性体ナノ粒子が良く機能すれば、画像化用抗体プローブの作成が簡便に行えるものと期待される。

一方，温度応答性リポソームについては、温度反応性に関する改良を行った。感温性リポソームは、体温環境下では薬物を保持するが、加温に応答して薬物を放出するリポソームである。これまでリン脂質のゲル－液晶転移を利用して温度応答性を付与したものが用いられていたが、応答温度の調節が困難であり、また、薬物放出の制御も不十分であった。本研究では、感温性高分子を複合化したリポソームを設計し、その抗癌剤の送達システムとしての機能を解析した。

B. 研究方法

a. 磁性体ナノ粒子の開発

本研究に使用する磁性体ナノ粒子は、目的の腫瘍組織に集中させるために、血中に長く滞留することが好ましい。即ち、血中半減期の長い特性を有する磁性体ナノ粒子の作成が必要要件となる。そこで、粒子表面上にカルボキシル基（陰性荷電）およびアミノ基（陽性荷電）を種々の割合で付与することにより、表面電荷の異なる粒子を作成するのに加えて、粒子サイズの調節を行うことで、本研究に最適な磁性体ナノ粒子を選定した。各磁性体ナノ粒子をマウスの尾静脈から投与したあと、経時的に血液を採取し、鉄含有量を NMR による T2 緩和時間を測定することにより、磁性体粒子の血中半減期を算出した。また、粒子表面に官能基を付与し、ペプチドを結合するための基点として使用した。

a. Z33 の発現／精製と磁性体ナノ粒子への結合

Z33 は報告されているアミノ酸配列をもとにオリゴ DNA を合成し、発現ベクターpTWIN1にクローニング後、大腸菌で発現させてキチンビーズにより精製した。同時に Z33 の N 末端あるいは C 末端にシステインをそれぞれ付加したペプチドを合成し、磁性体ナノ粒子にマレイミド基を介して結合させた。また、磁性体ナノ粒子 1 分子に結合させる Z33 のモル

Binding of 14-3-3β but not 14-3-3σ controls the cytoplasmic localization of CDC25B: binding site preferences of 14-3-3 subtypes and the subcellular localization of CDC25B

Sanae Uchida[1], Akiko Kuma[1,*], Motoaki Ohtsubo[2], Mari Shimura[3], Masato Hirata[4], Hitoshi Nakagama[5], Tsukasa Matsunaga[6], Yukihito Ishizaka[3] and Katsumi Yamashita[1,‡]

[1]Division of Life Science, Graduate School of Natural Science and Technology, Kanazawa University, Kakuma-machi, Kanazawa, 920-1192, Japan
[2]Institute of Life Science, Kurume University, Aikawa 2432-3, Kurume, 839-0861, Japan
[3]Division of Intractable Disease, International Medical Center of Japan, 21-1 Toyama 1-chome, Shinjuku-ku, Tokyo, 162-8655, Japan
[4]Laboratory of Molecular and Cellular Biochemistry, Faculty of Dental Science, and Station for Collaborative Research, Kyushu University, Maidashi, Fukuoka, 812-8582, Japan
[5]Biochemistry Division, National Cancer Center Research Institute, 1-1 Tsukiji 5-chome, Chuo-ku, Tokyo, 104-0045, Japan
[6]Laboratory of Molecular Human Genetics, Faculty of Pharmaceutical Sciences, Kanazawa University, 13-1 Takara-machi, Kanazawa, 920-0934, Japan
*Present address: Department of Cell Biology, National Institute for Basic Biology, 38 Nishigonaka, Myodaiji, Okazaki, 444-8585, Japan
‡Author for correspondence (e-mail: katsumi@kenroku.kanazawa-u.ac.jp)

Accepted 7 January 2004
Journal of Cell Science 117, 3011-3020 Published by The Company of Biologists 2004
doi:10.1242/jcs.01086

Summary

The dual specificity phosphatase CDC25B positively controls the G2-M transition by activating CDK1/cyclin B. The binding of 14-3-3 to CDC25B has been shown to regulate the subcellular redistribution of CDC25B from the nucleus to the cytoplasm and may be correlated with the G2 checkpoint. We used a FLAG-tagged version of CDC25B to study the differences among the binding sites for the 14-3-3 subtypes, 14-3-3β, 14-3-3ε and 14-3-3σ, and the relationship between subtype binding and the subcellular localization of CDC25B. All three subtypes were found to bind to CDC25B. Site-directed mutagenesis studies revealed that 14-3-3β bound exclusively near serine-309 of CDC25B1, which is within a potential consensus motif for 14-3-3 binding. By contrast, 14-3-3σ bound preferentially to a site around serine-216, and the presence of serine-137 and -309 enhanced the binding. In addition to these binding-site differences, we found that the binding of 14-3-3β drove CDC25B to the cytoplasm and that mutation of serine-309 to alanine completely abolished the cytoplasmic localization of CDC25B. However, co-expression of 14-3-3σ and CDC25B did not affect the subcellular localization of CDC25B. Furthermore, serine-309 of CDC25B was sufficient to produce its cytoplasmic distribution with co-expression of 14-3-3β, even when other putative 14-3-3 binding sites were mutated. 14-3-3ε resembled 14-3-3β with regard to its binding to CDC25B and the control of CDC25B subcellular localization. The results of the present study indicate that two 14-3-3 subtypes can control the subcellular localization of CDC25B by binding to a specific site and that 14-3-3σ has effects on CDC25B other than the control of its subcellular localization.

Key words: CDC25B, 14-3-3β, 14-3-3σ, Subcellular localization, G2 checkpoint

Introduction

The CDK (cyclin-dependent kinase) family of proteins controls the eukaryotic cell cycle, and one of these proteins, CDK1, is required for the onset and maintenance of mitosis. The activities of CDK family proteins related to cell cycle control are regulated by associations with cyclin proteins, interactions with cyclin-dependent kinase inhibitors, such as p21 and p27, and the phosphorylation-dephosphorylation cycle of CDK (Morgan, 1997). For instance, the phosphorylation of CDK1 at threonine-14 and tyrosine-15 by Wee1 and/or Myt1 kinases negatively controls CDK1 activity, whereas the dephosphorylation of CDK1 by the CDC25 family phosphatases activates CDK1, an essential step in the transition from G2 to M phase. The CDC25 family of dual protein phosphatases consists of three members, CDC25A, CDC25B, and CDC25C (Nilsson and Hoffman, 2000). CDC25A is thought to regulate the G1 to S transition, and CDC25B and C have been proposed to activate the CDK1/cyclin B1 complex to advance the cell cycle from G2 to M. Recent reports strongly suggest that CDC25A also has a function that is essential for the entry into and maintenance of M phase (Mailand et al., 2002).

The 14-3-3 family of proteins consists of small, acidic, highly conserved proteins that are present in all eukaryotic cells from yeast to mammals. There are seven isotypes present in mammalian cells. The 14-3-3 proteins are involved in numerous cellular processes related to signal transduction (Muslin and Xing, 2000; Tzivion et al., 2001; Yaffe, 2002).

These molecules bind to phosphoproteins at specific sequence motifs, which contain phosphoserine/threonine residues three amino acids downstream of an arginine (RxxS/T), and thereby regulate extracellular signaling or stress response pathways (Muslin et al., 1996; Yaffe et al., 1997). Emerging evidence suggests that 14-3-3 proteins are key regulators of cell cycle control, especially at cell cycle checkpoints, where they might function as negative regulators of DNA damage checkpoints. For example, one canonical 14-3-3 binding motif, which contains a phosphorylated serine residue, is similar to the consensus substrate motif of the checkpoint kinase Chk1 (Sanchez et al., 1997; Hutchins et al., 2000). In fission yeast, the 14-3-3 proteins Rad24/25 are required for checkpoint responses and are essential for cell survival (Ford et al., 1994). One of the 14-3-3 isotype proteins, 14-3-3σ is strongly up-regulated following genotoxic stress and is a downstream target of the tumor suppressor p53 (Hermeking et al., 1997).

The involvement of 14-3-3 in the progression from G2 to M was first suggested by the interactions of isolated 14-3-3β and ε with CDC25B (and CDC25A) and of isolated 14-3-3ζ with Wee1 (Conklin et al., 1995; Honda et al., 1997). Accumulated circumstantial evidence indicates that 14-3-3 negatively controls the G2-M transition by binding to these regulators. An association of 14-3-3 with human CDC25C was detected in G1, S and G2 phases, but not in M phase (Peng et al., 1997). The binding of 14-3-3 requires the Ser216 of CDC25C, and mutating this residue to Ala abolishes the interaction. This site is present in the potential recognition motif for 14-3-3 and is phosphorylated *in vitro* by checkpoint kinases, such as Chk1 and Chk2 (Sanchez et al., 1997; Peng et al., 1998; Matsuoka et al., 1998; O'Neill et al., 2002). Studies of the interaction between *Xenopus* CDC25C and 14-3-3 clearly demonstrated that the binding of 14-3-3 masks the nuclear localization signal of CDC25C, thereby causing nuclear exclusion of the protein without affecting its phosphatase activity (Kumagai et al., 1998; Kumagai and Dunphy, 1999; Yang et al., 1999). By contrast, the binding of 14-3-3 to *Xenopus* Wee1, after Chk1 activation by DNA damage or by stalled replication, augments Wee1 tyrosine kinase activity for CDK1 (Wang et al., 2000; Lee et al., 2001; Rothblum-Oviatt et al., 2001). Thus, the association of 14-3-3 with target proteins could modulate cell cycle progression through different mechanisms such as subcellular localization and enzyme activity, depending on cellular signaling.

In the normal cell cycle, CDC25B accumulates only at G2 phase and is degraded when cells exit M phase (Nagata et al., 1991; Galaktionov and Beach, 1991; Sebastian et al., 1993; Lammer et al., 1998). Interestingly, the overexpression of CDC25B induces a mitotic catastrophe by prematurely activating CDK1/cyclin B1, indicating that CDC25B induces mitosis more efficiently than CDC25C (Karlsson et al., 1999). In addition, the exogenous expression of CDC25B can override the G2 DNA damage checkpoint, and CDC25B is expressed in certain tumors (Miyata et al., 2001). Therefore, CDC25B has been proposed to be a potential oncogene acting to abrogate the DNA damage checkpoint (Galaktionov et al., 1995; Ma et al., 1999; Yao et al., 1999). Subcellular localization of CDC25B can be controlled by its association with 14-3-3 at a specific site on CDC25B2 or B3, Ser323 and might contribute to stall the cell cycle at the G2 phase following DNA damage (Mils et al., 2000; Davezac et al., 2000; Forrest and Babrielli, 2001). Ser323 of CDC25B2 or CDC25B3 (the equivalent to Ser309 of CDC25B1) is a crucial residue in the consensus 14-3-3 binding motif, where it is phosphorylated by the stress kinase p38 (Bulavin et al., 2001).

In the present study, we have analyzed the binding site specificity of three 14-3-3 subtypes, 14-3-3β, ε, and σ. Our results indicate that the binding site of 14-3-3σ differs markedly from those of 14-3-3β and 14-3-3ε. Moreover, the interaction of 14-3-3β or 14-3-3ε, but not of 14-3-3σ with CDC25B drives CDC25B from the nucleus into the cytoplasm. The biological significance of our results is discussed.

Materials and Methods

Cell culture and transfection

HEK293 cells (ATCC number CRL-1573) and U2OS cells (ATCC number HTB-96) were cultured in Dulbecco's modified Eagle's medium (DMEM) (Sigma, USA) supplemented with 10% fetal bovine serum (FBS) (Invitrogen, USA), 100 units/ml penicillin and 10 μg/ml streptomycin. Transient transfections were performed with FuGENE6 (Roche Diagnostics, Germany). For immunoprecipitation, cells were typically seeded at 1.3×10^6 per well. After 24 hours, cells were co-transfected with 2.5 μg of FLAG-tagged CDC25B and 1.0 μg of myc-tagged 14-3-3 DNA. For the indirect immunofluorescence experiments, cells were plated at a lower density, 2.0×10^5 per well and transfected after 24 hours with 3.0 μg of CDC25B DNA and 1.5 μg 14-3-3 of DNA. Transfected cells were processed for immunoblotting, immunoprecipitation, or immunostaining 24 hours after transfection. Leptomycin B, an inhibitor of CRM1 (exportin1), was obtained from Minoru Yoshida (RIKEN, Wako, Japan) and was administered to cells at a dose of 20 ng/ml to induce the nuclear accumulation of CDC25B.

Plasmids and site-directed mutagenesis

The cDNA of human CDC25B (CDC25B1 subtype), a kind gift from H. Okayama (University of Tokyo, Japan), was subcloned into the pEF6B vector (Invitrogen, USA) and expressed in transfected cells with a C-terminal FLAG tag. For point mutations at putative 14-3-3 binding sites, the following oligonucleotides (and their complements) were used to change serine to alanine (SA) in human CDC25B cDNA (CDC25B1). Clones with multiple mutations were generated by exchanging restriction fragments. The mutations were confirmed by sequencing.

S81A: 5′-CTGTCTCGACGGGCAGCCGAATCCTCCCTG-3′,
S137A: 5′-ATCAGACGCTTCCAGGCTATGCCGGTGAGG-3′,
S216A: 5′-GCCCAGAGACCCAGCGCGGCCCCCGACCTG-3′,
S309A: 5′-CTCTTCCGCTCTCCGGCCATGCCCTGCAGC-3′,
S361A: 5′-GTCCTCCGCTCAAAAGCACTGTGTCACGAT-3′.

The cDNAs of human 14-3-3β, ε, and σ were obtained by PCR amplification with the following oligonucleotides:

14-3-3β forward: 5′-ACTTGGAGTCAGCATATGACAATGGAT-3′,
14-3-3β reverse: 5′-CACTGGACGGATCCCAAAGCACGAGAA-3′,
14-3-3ε forward: 5′-GCCGCTGCCCATATGGATGATCGAGAG-3′,
14-3-3ε reverse: 5′-CTCTTGTGGGCGGATCCCTCACTGATT-3′,
14-3-3σ forward: 5′-GTCCCCAGACATATGGAGAGAGCCAGT-3′,
14-3-3σ reverse: 5′-GGTGGCGGGCAAGCTTCAGCTCTGGGG-CTC-3′.

PCR products were subcloned into the pEF6 vector. Each 14-3-3 cDNA was expressed in transfected cells in an N-terminal myc-tagged form.

Antibodies

Anti-FLAG M2 agarose was obtained from Sigma (USA). The rabbit

anti-FLAG antibody was described previously (Wang et al., 2001). Rabbit polyclonal and mouse monoclonal anti-myc-tag antibodies were purchased from Cell Signaling (USA). Antibodies to 14-3-3β (C-20), 14-3-3ε (T-16), and 14-3-3σ (N-14) were purchased from Santa Cruz Biotechnology (USA).

Preparation of crude cell extracts, immunoprecipitation and immunoblotting

Transfected cells were lysed in immunoprecipitation (IP) buffer (50 mM Tris-HCl pH 7.5, 150 mM NaCl, 0.5% NP-40, 5 mM EGTA, 1 mM EDTA) supplemented with a protease inhibitor mix and a phosphatase inhibitor mix. The protease inhibitor mix contained a 1:100 dilution of FOCUS protease arrest (Calbiochem, USA), 5 μg/ml E64 (Roche Diagnostics, Germany), 0.4 μM cathepsin inhibitor III (Sigma, USA), 10 μM MG132 (Calbiochem, USA), 20 μM N-acetyl-leu-leu-norleu-ala (Sigma, USA) and 1 mg/ml Pefabloc®SC (Roche Diagnostics, Germany). The phosphatase inhibitor mix consisted of a 1:100 dilution of Phosphatase inhibitor cocktail II (Sigma, USA), 20 mM *p*-nitrophenyl phosphate, 20 mM NaF, 20 mM β-glycerophosphate, 0.2 μM microcystin-LR (Calbiochem, USA), 0.2 μM calyculin A (Wako, Japan), 0.2 μM okadaic acid (Wako, Japan), 0.1 μM phenylarsin (Sigma, USA), and 0.2 μM cantharidin (Sigma, USA). FLAG-tagged CDC25B and mutant proteins were immunoprecipitated using FLAG M2-agarose; myc-tagged 14-3-3 proteins were immunoprecipitated with mouse monoclonal anti-myc tag antibody followed by protein G-Sepharose (Amersham Bioscience, USA). Cell lysates and immunoprecipitates were analyzed on western blots using rabbit polyclonal anti-FLAG (for CDC25B) or anti-myc antibodies (for exogenous 14-3-3), or 14-3-3 subtype-specific antibodies (for endogenous 14-3-3).

Indirect immunofluorescence microscopy

Transfected HEK293 cells grown on glass coverslips were fixed in 3.7% formaldehyde in PBS and then permeabilized with 0.5% Triton X-100 in PBS. FLAG-tagged CDC25B and mutants were detected with rabbit polyclonal anti-FLAG antibody and Alexa-594-conjugated goat anti-rabbit IgG (Molecular Probes, USA). Alternatively, myc-tagged 14-3-3 proteins were detected with mouse monoclonal anti-myc-tag antibody and Alexa-488-conjugated goat anti-mouse IgG (Molecular Probes, USA). In all samples, DNA was visualized with 4′,6-diamidino-2-phenylindole (DAPI) (Sigma, USA) at 0.1 μg/ml. To quantify the subcellular localization of CDC25B, more than 200 transfectant cells were counted and classified as having nuclear, diffuse or cytoplasmic localization.

Results

Binding of 14-3-3β, ε, and σ to CDC25B

Several groups have reported the interaction of 14-3-3 isotypes, such as 14-3-3β, ε, η, and ζ, with CDC25B (Mils et al., 2000; Forrest and Gabrielli, 2001). We have isolated 14-3-3β and ε as proteins that interact with CDC25B in yeast two-hybrid screening (S.U., A.K., M.O., M.S., M.H., H.N., T.M., Y.I. and K.Y., unpublished data), obtaining the same results as those previously reported (Conklin et al., 1995). Apart from these two 14-3-3 proteins (β and ε), 14-3-3σ was also reported to be possibly involved in a DNA damage checkpoint (Hermeking et al., 1997; Chan et al., 1999, 2000), which prompted us to isolate its cDNA and analyze its interaction with CDC25B.

We expressed FLAG-tagged CDC25B with myc-tagged 14-3-3β, ε or σ in HEK293 or U2OS cells and examined their interaction (Fig. 1). Expression of these proteins was confirmed in cell extracts prepared from transfected cells, as shown in Fig. 1 (Lysate). CDC25B was immunoprecipitated with anti-FLAG beads followed by western blotting and detection with either anti-FLAG or anti-myc antibody to detect CDC25B bound to 14-3-3. The results in Fig. 1 (IP: CDC25B) clearly indicate that all three 14-3-3 proteins can bind to CDC25B in co-transfected cells. To further confirm these results, reciprocal immunoprecipitation and western blot experiments were conducted in which CDC25B was detected in anti-myc immunoprecipitates of 14-3-3β, ε, or σ (Fig. 1, IP: 14-3-3). Thus, 14-3-3σ was most probably a new CDC25B-interacting protein.

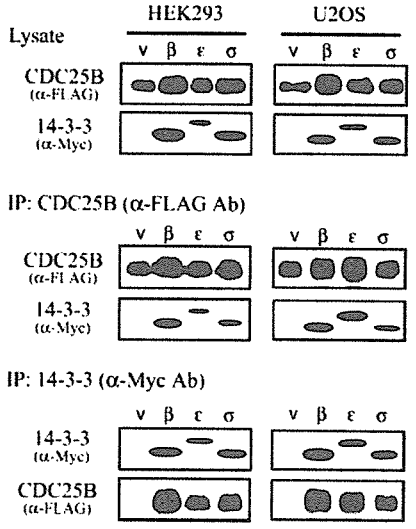

Fig. 1. 14-3-3β, 14-3-3ε, and 14-3-3σ bind to CDC25B in transfected cells. HEK293 (left panels) or U2OS (right panels) cells were transfected with FLAG-tagged CDC25B together with either empty vector or one of the myc-tagged 14-3-3 subtypes as described in Materials and Methods. (Top row) Lysate. Expression of CDC25B and 14-3-3- subtypes was confirmed in cell lysates with anti-FLAG antibody against CDC25B or anti-myc antibody against 14-3-3, respectively. (Middle row) IP: CDC25B (α-FLAG Ab). CDC25B was immunoprecipitated with anti-FLAG beads followed by western blotting and detection with anti-FLAG antibody to detect CDC25B and anti-myc antibody to detect CDC25B-bound 14-3-3. (Bottom row) IP: 14-3-3 (α-myc Ab. Reciprocal immunoprecipitation; CDC25B was detected in anti-myc immunoprecipitates. Protein 14-3-3 subtypes were immunoprecipitated with anti-myc antibody; the collected 14-3-3 or 14-3-3-bound CDC25B was detected by immunoblotting. v, empty vector; β, 14-3-3β, ε; 14-3-3ε, σ; 14-3-3σ.

Binding site specificity of 14-3-3 subtypes

The binding of 14-3-3 proteins to target proteins requires the specific motif RSxS/T(P)xP, where S/T(P) and x represent phosphoserine or phosphothreonine, and any amino acid, respectively (Muslin et al., 1996; Yaffe et al., 1997). The arginine (R) at position –3 from the phosphorylatable serine (or threonine) is a minimal requirement. In *Xenopus* for instance, after phosphorylation of CDC25 or Wee1 by Chk1 or other kinases, 14-3-3ε binds to the phosphorylated Ser287 in the RSPSMP sequence of CDC25 (Kumagai et al., 1998; Yang et al., 1999) and to the phosphorylated Ser549 in the RSVSFT sequence of Wee1 (Wang et al., 2000; Lee et al., 2001). There are several RxxS sites in CDC25B (or in our case, CDC25B1),

of which we chose the following five: 78-RRAS-81, 134-RFQS-137, 213-RPSS-216, 306-RSPS-309, and 358-RSKS-361, as shown in Fig. 2A. Of the relevant serine residues, Ser309 and Ser361 were phosphorylated by p38 in vitro and Ser309 was reported to be crucial for 14-3-3 binding after phosphorylation (Bulavin et al., 2001).

To analyze binding site specificity, we constructed three different groups of mutants in respect to the five above mentioned phosphorylatable serine sites of CDC25B1. Members of the first group have only a single mutation that changed one phosphorylatable serine to a non-phosphorylatable alanine; these mutants were namend CDC25B-S81A, S137A, etc. Members of the second group only remain a single phosphorylatable serine residue and contain mutations that changed the four serine residues to alanines; these mutants were named CDC25B-81S, 137S, etc. The only member of the last group is CDC25B-5SA in which all five serine residues were mutated to alanines. Using these mutants and the wild-type CDC25B, we determined the binding site specificity of 14-3-3β, ε, and σ.

Wild-type or mutant CDC25B were co-transfected with 14-3-3β, ε, or σ. Crude cell extracts were prepared, and expression of CDC25B and 14-3-3 was confirmed. Protein extracts were immunoprecipitated with anti-FLAG or anti-myc antibody, transferred for western blotting and detected with anti-myc or anti-FLAG antibody, respectively, to assess binding. We observed similar expression levels of CDC25B and 14-3-3 in transfected cells (Fig. 2B, Lysate), although lower levels of CDC25B mutants that failed to interact with 14-3-3, such as 81S and 5SA mutants, were occasionally detected (S.U., A.K., M.O., M.S., M.H., H.N., T.M., Y.I. and K.Y., unpublished data).

Interestingly, each 14-3-3 protein bound to a specific site on CDC25B (Fig. 2B, IP: CDC25B). These results clearly indicate that the CDC25B point mutation that changed Ser309 to Ala309, completely abolished 14-3-3β binding and that mutations of the other putative binding sites had essentially no effect on binding when compared with wild-type CDC25B. Also, experiments with the CDC25B mutant containing a single phosphorylatable serine revealed that Ser309 was the

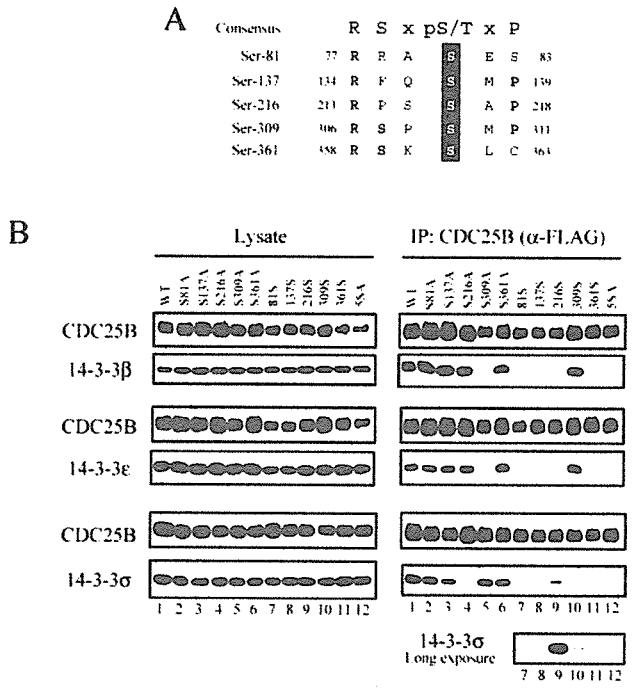

E

14-3-3	CDC25B mutants											
	WT	S81A	S137A	S216A	S309A	S361A	81S	137S	216S	309S	361S	5SA
14-3-3β	++	++	++	++	±	++	–	–	–	++	–	–
endo-14-3-3β	++	++	+	++	–	++	–	–	–	++	–	–
14-3-3ε	++	++	++	++	±	++				++		
endo-14-3-3ε	++	++	+	+	±	++	–	–	–	++	–	–
14-3-3σ	++	++	++	–	++	++	–	–	+	–	–	–
endo-14-3-3σ	++	++	+	–	++	++	–	–	+	–	–	–

Fig. 2. Binding of 14-3-3 subtypes to CDC25B is site specific. (A) Putative 14-3-3 consensus binding sites in CDC25B. (B-D) Mutants of CDC25B were transfected into HEK293 or U2OS cells either alone or together with 14-3-3 subtypes as indicated. Recovered CDC25B proteins are indicated (upper panel of each set of figures). The letters at the top and numbers at the bottom of each blot represent the CDC25B mutants: wild-type (1); S81A (2); S137A (3); S216A (4); S309A (5); S361A (6); 81S (7); 137S (8); 216S (9); 309S (10); 361S (11); 5SA (12). The definitions of the abbreviations for each mutant are described in the text. (B) Mutants of CDC25B were co-transfected into HEK293 cells with 14-3-3 subtypes β, ε or σ. Protein expression was determined by immunoblot. Wild-type or mutant CDC25B proteins were immunoprecipitated with anti-FLAG beads, and CDC25B-bound 14-3-3 was determined in the lysate (Lysate) and the immunoprecipitate [IP: CDC25B (α-FLAG Ab)]. Separate panel 'long exposure' shows 14-3-3 subtype σ after an exposure for 1 hour. (C) Mutants of CDC25B were transfected into HEK293 cells. Recovered CDC25B proteins and CDC25B-bound endogenous 14-3-3β (endo-14-3-3β) or endogenous 14-3-3ε (endo-14-3-3ε) were detected with specific antibodies in the lysate (Lysate) and the immunoprecipitate [IP: CDC25B (α-FLAG Ab]. (D) Mutants of CDC25B were transfected into U2OS cells. Recovered CDC25B and CDC25B-bound endogenous 14-3-3σ (endo-14-3-3σ) were detected with specific antibodies in the lysate (Lysate) and the immunoprecipitate [IP: CDC25B (α-FLAG Ab].(E) Binding of endogenous and transfected 14-3-3 subtypes to CDC25B mutants. ++, well bound; +, detectably bound; ±, faintly bound (could be detected only after long exposure); –, no binding.

sole site responsible for 14-3-3β binding. A faint signal was detected with the CDC25B mutants containing Ser137 or Ser216, but only after a long exposure time (S.U., A.K., M.O., M.S., M.H., H.N., T.M., Y.I. and K.Y., unpublished data). Exactly the same results were obtained for 14-3-3ε binding (Fig. 2B), i.e. the intact Ser309 fulfills the binding requirement. Surprisingly, entirely different results were obtained when 14-3-3σ was co-expressed with CDC25B. As shown in Fig. 2B, the mutation of Ser309 to Ala309 had little effect on 14-3-3σ binding. Instead, a single mutation changing Ser216 to Ala216 apparently abrogated the binding of 14-3-3σ. Experiments with single-serine constructs of CDC25B provided complementary results, indicating that only Ser216 is responsible for 14-3-3σ binding. Notice, that the amount of 14-3-3σ that bound to the CDC25B-S216 mutant was roughly half the amount of 14-3-3β or ε that bound to the CDC25B-S309 mutant. Therefore, the affinity of 14-3-3σ for Ser216 seems to be lower than those of 14-3-3β and ε for Ser309. Furthermore, 14-3-3σ bound to two other binding sites, Ser137 and Ser309, although with a lower affinity than the binding to Ser216 (Fig. 2B, Long exposure).

Binding of endogenous 14-3-3 to CDC25B

Next, we addressed the question of whether endogenous 14-3-3 binds to transfected CDC25B. After transfection of wild-type or mutant CDC25B, CDC25B was recovered and CDC25-bound 14-3-3β, ε, or σ was detected with subtype-specific antibodies. CDC25B was transfected to HEK293 cells to investigate binding of 14-3-3β and ε. U2OS cells were used to determine 14-3-3σ binding because no expression of 14-3-3σ was detected in HEK293 cells. Binding of endogenous 14-3-3β and ε is shown in Fig. 2C and that of 14-3-3σ in Fig. 2D. As illustrated, the results were essentially the same as those for the exogenously expressed ones. 14-3-3β and ε preferentially bound to Ser309 and a mutation to Ala at this site impaired 14-3-3 binding. Unlike 14-3-3β and ε, a Ser to Ala mutation at Ser216 eliminated 14-3-3σ binding (summarized in Fig. 2E). As clearly indicated, both endogenous and exogenous 14-3-3β and ε preferentially bind to Ser309, whereas 14-3-3σ prefers Ser216. Besides these two sites, Ser137 seems to be a favored binding site for the three 14-3-3 subtypes tested here because the binding signals are reduced by mutation at Ser137 (Fig. 2C and D). In respect to the other putative binding sites, we found no evidence that the 14-3-3 subtypes bind to either Ser81 or Ser361.

Multiple binding sites for 14-3-3σ on CDC25B

The results shown in Fig. 2 suggest that 14-3-3σ binds to CDC25B at multiple sites and possibly requires two sites to stably bind the protein. To explore this further, we constructed a series of mutants in which two serine residues were changed to alanine, and examined the binding of the 14-3-3 subtypes (Fig. 3). Compared with the single SA mutant (i.e. S216A), binding of 14-3-3σ to double SA mutants, such as S216/309A, was weaker or absent. Further work with the double mutants indicated that either of two sites, Ser137 or Ser309, seem to work cooperatively with Ser216. These results strongly suggest that 14-3-3σ requires two sites, Ser216 and Ser137 or Ser216 and Ser309, to interact effectively with CDC25B, and that 14-3-3σ might function as a dimer.

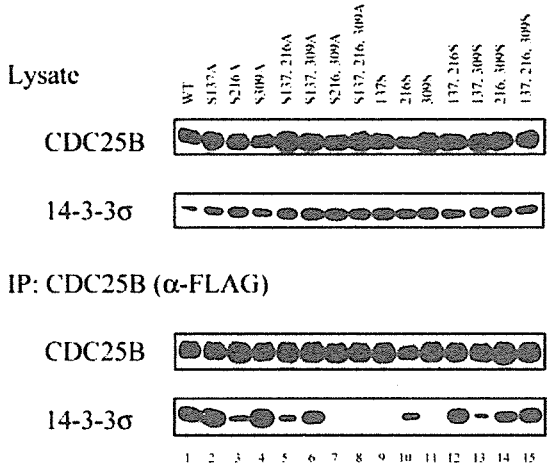

Fig. 3. Efficient binding of 14-3-3σ to CDC25B requires two independent sites. HEK293 cells were co-transfected with 14-3-3σ and a series of CDC25B mutants. Protein expression (Lysate) and protein binding (IP: CDC25B (α-FLAG Ab)) were detected. The letters in the upper panel of Lysate indicate CDC25B wild type and respective mutants. The definitions of the abbreviations for each mutant are described in the text.

14-3-3 binding sites and subcellular localization of CDC25B

Binding of 14-3-3 to CDC25B was previously reported to induce the redistribution of CDC25B from the nucleus to the cytoplasm; the amino acid residue essential for this effect was shown to be Ser323 of CDC25B3 (or CDC25B2), which corresponds to Ser309 of CDC25B1 in our experiments (Davezac et al., 2000; Forrest and Gabrielli, 2001). Therefore, we analyzed the subcellular localization of CDC25B mutants expressed in combination with 14-3-3 subtypes that possess different binding site preferences. To assess the effects of co-transfection on the subcellular localization of CDC25B, we distinguished three different distributions [nuclear (N), diffuse (N=C) and cytoplasmic (C)] of CDC25B (Fig. 4A). The localization of exogenously expressed CDC25B was mainly nuclear (Fig. 4B), transfected 14-3-3β or σ was detected in the cytoplasm (S.U., A.K., M.O., M.S., M.H., H.N., T.M., Y.I. and K.Y., unpublished data). Upon co-transfection with 14-3-3β, CDC25B exhibited a diffuse distribution (Fig. 4B). Quantitatively, the percentage of cells with nuclear CDC25B was reduced from 55% to 30% and that of cells with a diffuse distribution increased from 38% to 60% when co-expressed with 14-3-3β. Based on our results, it is possible that nuclear localization is disturbed by 14-3-3 binding. Interestingly, the expression of 14-3-3σ had no effect on the localization of CDC25B. These results led us to hypothesize that when 14-3-3β binds to Ser309 of CDC25B, it can drive CDC25B from the nucleus to the cytoplasm, but that 14-3-3σ, which does not bind primarily to Ser309, has no ability to do so.

Effects of mutations at 14-3-3 binding sites on the localization of CDC25B

The primary 14-3-3β binding site on CDC25B was Ser309, and a point mutation at this site that changed serine to alanine abolished the interaction. If the binding of 14-3-3β is correlated

with the cytoplasmic localization of CDC25B, 14-3-3β could not drive the CDC25B mutant out of the nucleus. The results shown in Fig. 4C indicate that the mutation Ser309 to Ala309 in CDC25B completely disrupted its cytoplasmic localization with more than 90% of the mutant protein being located in the nuclei. In contrast to the wild type, this CDC25B mutant was not diffused into the cytoplasm by co-expression of 14-3-3β or 14-3-3σ. However, mutant S216A behaved like the wild type, i.e. its subcellular localization was effectively changed from nuclear to diffuse when co-expressed with 14-3-3β (Fig. 4D). Moreover, introduction of 14-3-3σ did not cause any change in the distribution of CDC25B. Collectively, these results show that Ser309 is essential for the cytoplasmic distribution of CDC25B and that Ser216 does not have any influence on the subcellular localization of CDC25B, even when 14-3-3σ binds to it.

To confirm that the subcellular distribution of CDC25B by 14-3-3β depends on Ser309, we made mutants in which serine was changed to alanine at four of the five sites that have a single phosphorylatable serine residue. The mutants were denoted as CDC25B-81S, CDC25B-137S, CDC25B-216S, CDC25B-309S and CDC25B-361S (as mentioned in Fig. 2). These CDC25B mutants were transfected with or without 14-3-3 and their localizations analyzed. Only CDC25B-309S behaved like the wild type (Fig. 5B); the other mutants exhibited nuclear localizations, probably because they possessed the S309A mutation and could not bind to 14-3-3β (Fig. 5A). Wild-type CDC25B and the CDC25B-309S mutant exhibited nuclear localization in about 60% of the cells (Fig. 5B). As was the case with wild-type CDC25B (see Fig. 4B), the expression of 14-3-3β antagonized the nuclear localization of CDC25B-309S and led to a diffuse distribution (Fig. 5B). In contrast to 14-3-3β, 14-3-3σ did not bind to the mutant and had no effect on the nuclear localization of CDC25B-309S or wild-type CDC25B (Fig. 5B). These results strongly suggest that only Ser309 of CDC25B is required for the control of the subcellular localization of CDC25B by 14-3-3β.

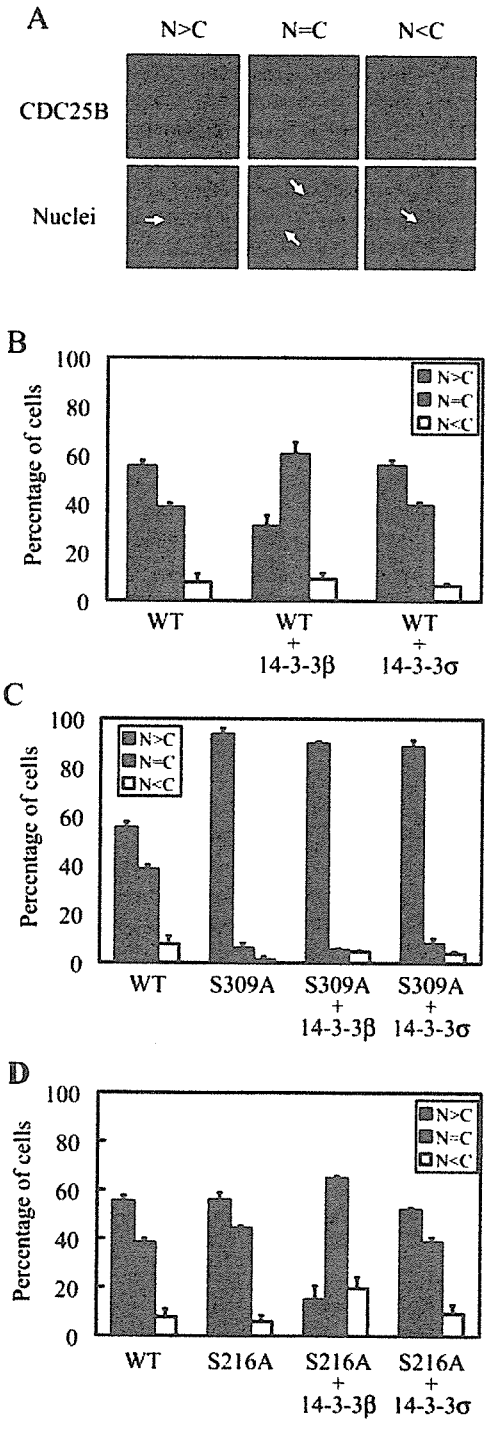

Effects of 14-3-3ε on the nuclear localization of CDC25B

The results shown in Fig. 2 indicate that Ser309 of CDC25B is the specific binding site for 14-3-3ε. We examined the effects

Fig. 4. 14-3-3β but not 14-3-3σ efficiently redistributes CDC25B from the nucleus to the cytoplasm. HEK293 cells were transfected with FLAG-tagged CDC25B in combination with empty vector, myc-tagged 14-3-3β or myc-tagged 14-3-3σ, followed by immunostaining with anti-FLAG antibodies to detect the subcellular localization of CDC25B and with anti-myc antibodies to detect co-transfected 14-3-3 proteins. Analyses showed that more than 95% of the cells that expressed CDC25B also expressed the co-transfected 14-3-3 proteins. (A) Exemplary images, showing how the subcellular distribution of CDC25B was evaluated: N>C, predominantly nuclear; N=C diffuse; N<C, predominantly cytoplasmic. (B) Wild-type CDC25B was co-transfected with empty vector (WT), myc-tagged 14-3-3β (WT+14-3-3β) or myc-tagged 14-3-3σ (WT+14-3-3σ) to quantify the subcellular distribution of CDC25B. Over 200 cells expressing CDC25B were counted to determine the percentage of cells that express CDC25B with nuclear, diffuse and cytoplasmic distribution. Error bars in graphs represent the means±s.d. of three independent experiments. (C) Transfection with wild-type CDC25B alone (WT), S309A mutant of CDC25B alone (S309A) and mutant S309A in combination with myc-tagged 14-3-3β (S309A+14-3-3β) or myc-tagged 14-3-3σ (S309A+14-3-3σ). Over 200 cells expressing CDC25B were counted to determine the percentage of cells that express CDC25B with nuclear, diffuse and cytoplasmic distribution. Error bars in graphs represent the means±s.d. of three independent experiments. (D) Transfection with wild-type CDC25B alone (WT), S216A mutant of CDC25B alone (S216A) and mutant S216A in combination with myc-tagged 14-3-3β (S216A+14-3-3β) or myc-tagged 14-3-3σ (S216A+14-3-3σ). Over 200 cells expressing CDC25B were counted to determine the percentage of cells that express CDC25B with nuclear, diffuse and cytoplasmic distribution. Error bars in graphs represent the means±s.d. of three independent experiments.

of 14-3-3ε on the subcellular localization of CDC25B in three sets of experiments. First, 14-3-3ε was co-transfected with wild-type CDC25B and CDC25B-distribution (as defined above and in Fig. 4A) was analyzed by counting the cells. Co-expression of 14-3-3ε reduced the percentage of cells with nuclear localization of CDC25B from 55% to 47% and concomitantly increased the percentage of cells displaying a diffuse pattern from 40% to 55% (Fig. 6A). Second, 14-3-3ε was co-transfected with the CDC25B-309S mutant. Here, the nuclear localization of CDC25B decreased from 60% to 37%, whereas its diffuse distribution increased from 35% to 55% (Fig. 6B). We found no effects of the co-expression of 14-3-3ε on the subcellular localization of the CDC25B-S309A mutant (Fig. 6C). In summary, the results with 14-3-3ε were exactly the same as those obtained with 14-3-3β and different from those with 14-3-3σ.

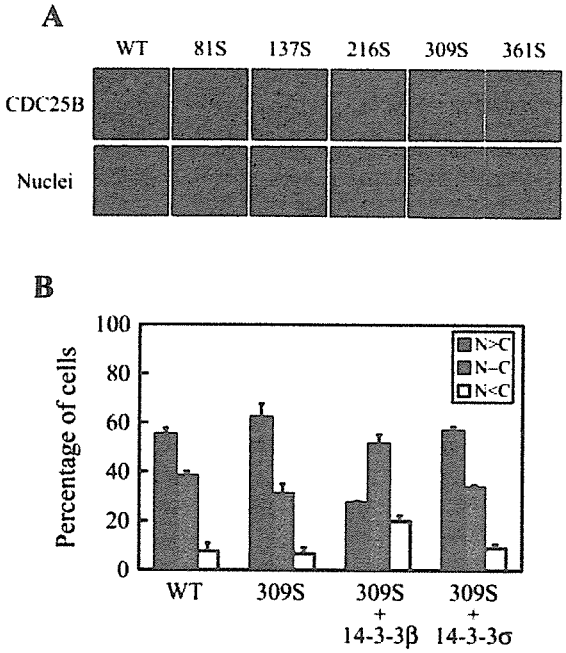

Fig. 5. Only the 309S mutant of CDC25B was distributed diffusely with co-transfection of 14-3-3β. (A) Wild type CDC25B or different CDC25B mutants with a single phosphorylatable serine were co-transfected with 14-3-3β into HEK293 cells. (Upper panels) Subcellular localization of CDC25B wild type and mutants. (Lower panel) Corresponding images of nuclei. (B) Percentage of cells transfected with mutant CDC25B 309S (shown in A) that express CDC25B with nuclear, diffuse and cytoplasmic distribution. Over 200 cells expressing CDC25B were counted to determine the percentage of cells that express CDC25B. Transfection with wild-type CDC25B alone (WT), 309S mutant of CDC25B alone (309S) and mutant 309S in combination with myc-tagged 14-3-3β (309S +14-3-3β) or myc-tagged 14-3-3σ (309S +14-3-3σ). Error bars in graphs represent the means±s.d. of three independent experiments. Subcellular distribution of CDC25B: N>C, predominantly nuclear; N=C diffuse; N<C, predominantly cytoplasmic (C).

Effects of 14-3-3β binding on the nuclear import of CDC25B

Several previous studies demonstrated that treating cells with leptomycin B (LMB), a CRM1 (exportin1) inhibitor, disrupts the cytoplasmic localization of CDC25B (Nishi et al., 1994; Kudo et al., 1998; Karlsson et al., 1999; Davezac et al., 2000) (Fig. 7A). Therefore, it might be that 14-3-3β-binding slows down the nuclear import of CDC25B by LMB. After transfecting CDC25B with or without 14-3-3β, cells were treated with LMB and the nuclear accumulation of CDC25B was measured. As shown in Fig. 7B, co-expression of exogenous 14-3-3β efficiently inhibited the nuclear import of CDC25B. Notice that this effect was not observed when 14-3-3σ was co-transfected with CDC25B. These results suggest that 14-3-3β masks the nuclear localizing signal (NLS) of CDC25B, which is located about 30 amino acids downstream of Ser309.

Discussion

It has long been believed that higher eukaryotic cells have two dual specificity phosphatases, CDC25B and CDC25C, which activate CDK1/cyclin B to initiate mitosis. Recent reports indicate that another dual specificity phosphatase, CDC25A, plays a crucial role in G2-M events (Mailand et al., 2002). CDC25A can bind and activate CDK1/cyclin B, and downregulation by RNAi delays mitotic entry. In addition, the overexpression of CDC25A abrogates the G2 DNA-damage checkpoint (Mailand et al., 2002; Chow et al., 2003). Therefore, it is possible to regard CDC25A as a master activator of CDK/cyclin in the cell cycle, and the roles of

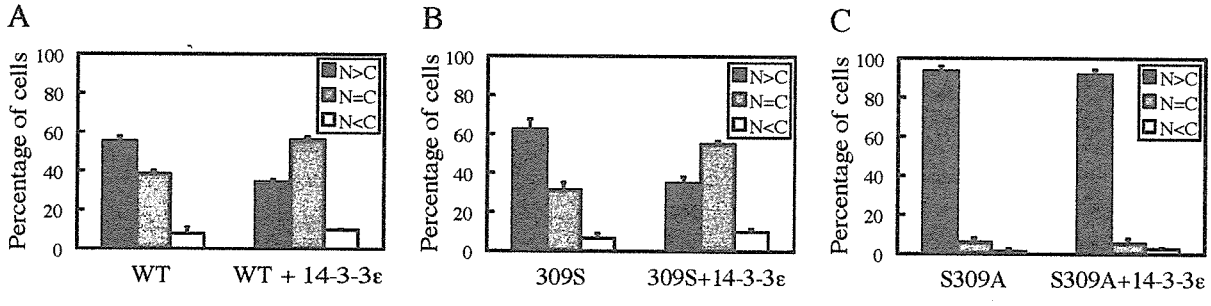

Fig. 6. 14-3-3ε had effects similar to those of 14-3-3β on the subcellular localization of CDC25B. HE293 cells were transfected with (A) wild-type CDC25B, (B) the 309S mutant or (C) the S309A mutant with or without 14-3-3ε. Over 200 cells expressing CDC25B were counted to determine the percentage of cells that express CDC25B with nuclear, diffuse and cytoplasmic distribution. Error bars in graphs represent the means±s.d. of three independent experiments. Subcellular distribution of CDC25B: N>C, predominantly nuclear; N=C diffuse; N<C, predominantly cytoplasmic (C).

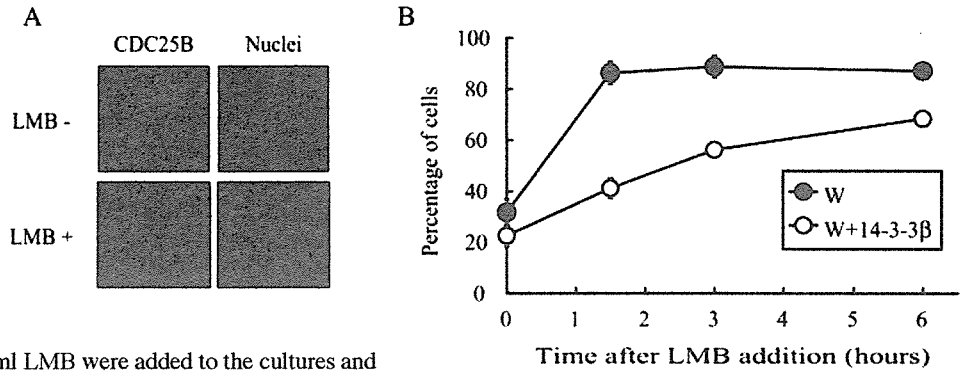

Fig. 7. Binding of 14-3-3β to CDC25B efficiently slowed down the nuclear import of CDC25B induced by leptomycin B (LMB). (A) HEK293 cells transfected with wild-type CDC25B and treated with 20 ng/ml LMB at for 3 hours. Transfected CDC25B was detected with anti-FLAG antibody. The upper and lower panels show the results without or with LMB treatment, respectively. (B) HEK293 cells transfected with wild-type CDC25B alone or with 14-3-3β. Twenty-four hours after transfection, 20 ng/ml LMB were added to the cultures and the percentage of cells exhibiting nuclear-specific localization of CDC25B was determined at the indicated time-points: 0 (before addition of LMB), 1.5, 3 or 6 hours after the addition. Over 200 cells expressing CDC25B were counted to determine the percentage of cells that express CDC25B. The percentage of cells with a nuclear localization (as shown in Fig. 4) was determined from three independent experiments. ●, CDC25B; ○,CDC25B with 14-3-3β.

CDC25B and CDC25C as being restricted to G2-M events to activate CDK1/cyclin B.

It has been proposed that CDC25C inhibits human CDC25C, by downregulating its phosphatase activity or by binding 14-3-3 after the phosphorylation of Ser216 (Peng et al., 1997; Blasina et al., 1999; Furnari et al., 1999; Graves et al., 2001). The amount of cellular CDC25C is essentially kept constant. Therefore, a qualitative regulation of its functions, i.e. enzyme activity and subcellular localization, is required to control cell cycle progression. In the case of CDC25B, the protein accumulates as the cell cycle progresses, reaching a maximum at G2-M phase. Thus, controlling the expression of CDC25B is an effective means of regulating its function. However, at G2 phase, when the CDC25B level is at its peak, an alternate way of keeping it inactive is needed when its activation is inappropriate. Recently, several groups have reported that the binding of 14-3-3, specifically at Ser309 of CDC25B1 or Ser323 of CDC25B2 or CDC25B3, results in the cytoplasmic localization of CDC25B, supporting the theory of its redistribution from the nucleus to the cytoplasm as a critical G2-M checkpoint (Davezac et al., 2000; Forrest and Gabrielli, 2001).

In agreement with these reports, we found that 14-3-3β and 14-3-3ε bound specifically at Ser309 of CDC25B1 and that the binding effectively redistributed CDC25B, decreasing its amount in the nuclei. We consistently detected nuclear localization in about 50% of the CDC25B-transfected cells. Endogenous 14-3-3, detected with a pan-14-3-3 antibody, was recovered as a complex with exogenous CDC25B. The co-expression of 14-3-3β or 14-3-3ε reduced the nuclear localization of exogenous CDC25B by about 20%, but endogenous 14-3-3 was recovered with exogenous CDC25B. More than 95% of the introduced CDC25B was localized in nuclei when the binding of 14-3-3 was abolished by a CDC25B point mutation. Thus, it is reasonable to conclude that the binding of 14-3-3 at Ser309 of CDC25B is essential for the exclusion of CDC25B from the nucleus. We also presented evidence that binding of 14-3-3β to CDC25B slowed down the nuclear import induced by LMB treatment. Since 14-3-3β specifically binds to Ser309, bound 14-3-3 should impair the access of nuclear import cargos, such as importin, to the NLS.

In *Xenopus*, 14-3-3-binding to CDC25C was suggested to mask its NLS, making its nuclear exclusion signal (NES) available for the transfer of CDC25C to the cytoplasm (Kumagai and Dunphy, 1999). The NLS in human CDC25B is located at the same position relative to the 14-3-3-binding site of CDC25C in Xenopus, i.e., about 30 amino acids downstream of Ser309 (Davezac et al., 2000) (S.U., A.K., M.O., M.S., M.H., H.N., T.M., Y.I. and K.Y., unpublished data). Therefore, the binding of 14-3-3β or 14-3-3ε at Ser309 could inactivate the NLS, which in turn would make the N-terminal NES dominant. This idea is further supported by the observation that the preferential binding of 14-3-3σ to Ser216 does not cause cytoplasmic redistribution of CDC25B because Ser216 is too far away to allow 14-3-3σ to mask the NLS. We also conclude from this result that the NES-like sequence present in the C-terminus of all 14-3-3 subtypes does not function as an NES. Thus, our results agree well with the recently presented hypothesis that the binding of 14-3-3 does not add an 'attachable NES' that targets proteins (Rittinger et al., 1999; Brunet et al., 2002). Instead, it might serve other functions, such as providing scaffolding or a cover that hides specific motifs, such as NLS or NES (Muslin and Xing, 2000; Tzivion et al., 2001; Yaffe, 2002).

Ser309 was shown to be phosphorylated by p38 MAP kinase, and the kinase activity was necessary to maintain cell cycle arrest at G2 in response to DNA damage caused by UV light (Bulavin et al., 2001). One of the checkpoint kinases, Chk1, can phosphorylate Ser309 to enhance 14-3-3-binding in vitro (Forrest and Gabrielli, 2001) (S.U., A.K., M.O., M.S., M.H., H.N., T.M., Y.I. and K.Y., unpublished data). Although co-expression of MKK6, Chk1 or Chk2 with CDC25B and 14-3-3β enhanced the binding of 14-3-3β to CDC25B, these effects were not significant (S.U., A.K., M.O., M.S., M.H., H.N., T.M., Y.I. and K.Y., unpublished data). Therefore, Ser309 seems to be constitutively phosphorylated, possibly by p38 or C-TAK1. If phosphorylation of this serine is crucial for the induction and/or maintenance of G2 arrest, the inactivation of the phosphatase responsible for the dephosphorylation might also occur, although enhanced checkpoint kinase activity is usually thought to maintain the phosphorylation state. The significance of the cytoplasmic localization of CDC25B in terms of cell cycle regulation, especially at the G2 checkpoint, is not clear. However, abrogation of the 14-3-3 binding site

abolished G2-arrest and thus caused localization of CDC25B to the nucleus. The overexpression of CDC25B is sufficient to override the G2 DNA damage checkpoint (Miyata et al., 2001), but in this case, Ser309 of the overexpressed CDC25B would be phosphorylated as is the endogenous residue. In addition, the amount of cellular 14-3-3 is obviously in excess of the amount of CDC25B, and thus the equilibrium between 14-3-3-bound CDC25B and unbound CDC25B should be the same in transfected cells and in normal cells. If overexpression enhances the probability of the localization of CDC25B in the nucleus, CDC25B could counteract the inhibitory effects of Wee1 kinase, leading to the activation of CDK1/cyclin B and abrogation of the G2 checkpoint. Phosphorylation of Ser309 should be necessary to inhibit premature mitosis, but it is too early to attribute maintained phosphorylation at the G2 checkpoint to the checkpoint kinases or to p38. So, if Ser309 is constantly phosphorylated, then its phosphorylation level could never be enhanced because of DNA damage (Bulavin et al., 2001). Indeed, no reports indicate a higher than normal phosphorylation level of Ser309 or Ser323 in CDC25B2 or CDC25B3 at the G2 checkpoint, although it is possible to postulate a change from the maintenance kinases to the checkpoint kinases at the checkpoint state to keep the phosphorylation level constant (Bulavin et al., 2002). Thus, the significance of the phosphorylation of Ser309, in combination with the binding of 14-3-3 at the site, must await further conclusions about the G2 checkpoint.

We have reported here the binding of 14-3-3σ at Ser216 of CDC25B, which has not been reported previously. We have also described another site, Ser137, that seems to provide support for the binding of 14-3-3σ. The subtypes 14-3-3β and ε have little preference for either of these sites, although both serine residues partly satisfy the consensus-binding motif of 14-3-3 (RxxS). It is rare to find binding-preference differences among 14-3-3 subtypes and it should be noticed that 14-3-3σ does not prefer Ser309 for binding even though it is in one of the typical 14-3-3 binding motifs. Interestingly, 14-3-3σ also does not bind to CDC25C where Ser216 is located in a typical 14-3-3 binding motif (RSxSMP) (Chan et al., 1999) (S.U., A.K., M.O., M.S., M.H., H.N., T.M., Y.I. and K.Y., unpublished data). Two sites on CDC25B are required for the efficient binding of 14-3-3σ, which means that 14-3-3σ must be a dimer to bind efficiently to the two different sites on CDC25B.

During the preparation of this manuscript an on-line report was published, describing two sites, other than Ser323 of CDC25B2, necessary for 14-3-3 binding (Giles et al., 2003). Those two sites in CDC25B2, Ser151 and Ser230, are exactly the same as Ser137 and Ser216 of CDC25B1 that have been discussed here. We have demonstrated that 14-3-3σ binds to these sites. It is well known that 14-3-3σ is one of the downstream transcriptional targets of p53 (Hermeking et al., 1997). There have been several reports that 14-3-3σ can downregulate CDK activity by binding to it or that 14-3-3σ can move the CDK1/cyclin B complex to the cytoplasm (Bulavin et al., 2002). Here, we suggest that 14-3-3σ downregulates the function of CDC25B and thereby acts as a G2-checkpoint regulator. Our preliminary experiments indicate that the co-expression of CDC25B and Chk1, but not MKK6 (that activates p38), enhances phosphorylation at Ser137 and Ser216 (S.U., A.K., M.O., M.S., M.H., H.N., T.M., Y.I. and K.Y., unpublished data). Further studies are required to determine whether the phosphorylation of both sites leads to the binding of 14-3-3σ and to establish the consequences for CDC25B.

We thank Hiroto Okayama (University of Tokyo) and Minoru Yoshida (RIKEN) for the generous gift of CDC25B1 cDNA and leptomycin B, respectively. This work was supported in part by Grants-in-Aid for Scientific Research (to K.Y. and Y.I.) and for the Second Term of the Comprehensive 10-Year Strategy for Cancer Control (to H.N.) from the Ministry of Health, Labor, and Welfare of Japan.

References

Blasina, A., de Weyer, I. V., Laus, M. C., Luyten, W. H., Parker, A. E. and McGowan, C. H. (1999). A human homologue of the checkpoint kinase Cds1 directly inhibits Cdc25 phosphatase. *Curr. Biol.* **9**, 1-10.

Brunet, A., Kanai, F., Stehn, J., Xu, J., Sarbassova, D., Frangioni, J. V., Dalal, S. N., DeCaprio, J. A., Greenberg, M. E. and Yaffe, M. B. (2002). 14-3-3 transits to the nucleus and participates in dynamic nucleocytoplasmic transport. *J. Cell Biol.* **156**, 817-828.

Bulavin, D. V., Higashimoto, Y., Popoff, I. J., Gaarde, W. A., Basrur, V., Potapova, O., Appella, E. and Fornace, A. J. Jr (2001). Initiation of a G2/M checkpoint after ultraviolet radiation requires p38 kinase. *Nature* **411**, 102-107.

Bulavin, D. V., Amundson, S. A. and Fornace, A. J. (2002). p38 and Chk1 kinases: different conductors for the G(2)/M checkpoint symphony. *Curr. Opin. Genet. Dev.* **12**, 92-97.

Chan, T. A., Hermeking, H., Lengauer, C., Kinzler, K. W. and Vogelstein, B. (1999). 14-3-3Sigma is required to prevent mitotic catastrophe after DNA damage. *Nature* **401**, 616-620.

Chan, T. A., Hwang, P. M., Hermeking, H., Kinzler, K. W. and Vogelstein, B. (2000). Cooperative effects of genes controlling the G(2)/M checkpoint. *Genes Dev.* **14**, 1584-1588.

Chow, J. P., Siu, W. Y., Fung, T. K., Chan, W. M., Lau, A., Arooz, T., Ng, C. P., Yamashita, K. and Poon, R. Y. (2003). DNA damage during the spindle-assembly checkpoint degrades CDC25A, inhibits cyclin-CDC2 complexes, and reverses cells to interphase. *Mol. Biol. Cell* **14**, 3989-4002.

Conklin, D. S., Galaktionov, K. and Beach, D. (1995). 14-3-3 proteins associate with cdc25 phosphatases. *Proc. Natl. Acad. Sci. USA* **92**, 7892-7896.

Davezac, N., Baldin, V., Gabrielli, B., Forrest, A., Theis-Febvre, N., Yashida, M. and Ducommun, B. (2000). Regulation of CDC25B phosphatases subcellular localization. *Oncogene* **19**, 2179-2185.

Ford, J. C., al-Khodairy, F., Fotou, E., Sheldrick, K. S., Griffiths, D. J. and Carr, A. M. (1994). 14-3-3 protein homologs required for the DNA damage checkpoint in fission yeast. *Science* **265**, 533-535.

Forrest, A. and Gabrielli, B. (2001). Cdc25B activity is regulated by 14-3-3. *Oncogene* **20**, 4393-4401.

Furnari, B., Blasina, A., Boddy, M. N., McGowan, C. H. and Russell, P. (1999). Cdc25 inhibited in vivo and in vitro by checkpoint kinases Cds1 and Chk1. *Mol. Biol. Cell.* **10**, 833-845.

Galaktionov, K. and Beach, D. (1991). Specific activation of cdc25 tyrosine phosphatases by B-type cyclins: evidence for multiple roles of mitotic cyclins. *Cell* **67**, 1181-1194.

Galaktionov, K., Lee, A. K., Eckstein, J., Draetta, G., Meckler, J., Loda, M. and Beach, D. (1995). CDC25 phosphatases as potential human oncogenes. *Science* **269**, 1575-1577.

Giles, N., Forrest, A. and Gabrielli, B. (2003). 14-3-3 acts as an intramolecular bridge to regulate cdc25B localization and activity. *J. Biol. Chem.* **278**, 28580-28587.

Graves, P. R., Lovly, C. M., Uy, G. L. and Piwnica-Worms, H. (2001). Localization of human Cdc25C is regulated both by nuclear export and 14-3-3 protein binding. *Oncogene* **20**, 1839-1851.

Hermeking, H., Lengauer, C., Polyak, K., He, T. C., Zhang, L., Thiagalingam, S., Kinzler, K. W. and Vogelstein, B. (1997). 14-3-3 sigma is a p53-regulated inhibitor of G2/M progression. *Mol. Cell* **1**, 3-11.

Honda, R., Ohba, Y. and Yasuda, H. (1997). 14-3-3 zeta protein binds to the carboxyl half of mouse wee1 kinase. *Biochem. Biophys. Res. Commun.* **230**, 262-265.

Hutchins, J. R., Hughes, M. and Clarke, P. R. (2000). Substrate specificity determinants of the checkpoint protein kinase Chk1. *FEBS Lett.* **466**, 91-95.

Karlsson, C., Katich, S., Hagting, A., Hoffmann, I. and Pines, J. (1999). Cdc25B and Cdc25C differ markedly in their properties as initiators of mitosis. *J. Cell. Biol.* **146**, 573-584.

Kudo, N., Wolff, B., Sekimoto, T., Schreiner, E. P., Yoneda, Y., Yanagida, M., Horinouchi, S. and Yoshida, M. (1998). Leptomycin B inhibition of signal-mediated nuclear export by direct binding to CRM1. *Exp. Cell Res.* **242**, 540-547.

Kumagai, A. and Dunphy, W. G. (1999). Binding of 14-3-3 proteins and nuclear export control the intracellular localization of the mitotic inducer Cdc25. *Genes Dev.* **13**, 1067-1072.

Kumagai, A., Yakowec, P. S. and Dunphy, W. G. (1998). 14-3-3 proteins act as negative regulators of the mitotic inducer Cdc25 in Xenopus egg extracts. *Mol. Biol. Cell* **9**, 345-354.

Lammer, C., Wagerer, S., Saffrich, R., Mertens, D., Ansorge, W. and Hoffmann, I. (1998). The cdc25B phosphatase is essential for the G2/M phase transition in human cells. *J. Cell Sci.* **111**, 2445-2453.

Lee, J., Kumagai, A. and Dunphy, W. G. (2001). Positive regulation of Wee1 by Chk1 and 14-3-3 proteins. *Mol. Biol. Cell* **12**, 551-563.

Ma, Z. Q., Chua, S. S., DeMayo, F. J. and Tsai, S. Y. (1999). Induction of mammary gland hyperplasia in transgenic mice over-expressing human Cdc25B. *Oncogene* **18**, 4564-4576.

Mailand, N., Podtelejnikov, A. V., Groth, A., Mann, M., Bartek, J. and Lukas, J. (2002). Regulation of G2/M events by Cdc25A through phosphorylation-dependent modulation of its stability. *EMBO J.* **21**, 5911-5920.

Matsuoka, S., Huang, M. and Elledge, S. J. (1998). Linkage of ATM to cell cycle regulation by the Chk2 protein kinase. *Science* **282**, 1893-1897.

Mils, V., Baldin, V., Goubin, F., Pinta, I., Papin, C., Waye, M., Eychene, A. and Ducommun, B. (2000). Specific interaction between 14-3-3 isoforms and the human CDC25B phosphatase. *Oncogene* **19**, 1257-1265.

Miyata, H., Doki, Y., Yamamoto, H., Kishi, K., Takemoto, H., Fujiwara, Y., Yasuda, T., Yano, M., Inoue, M., Shiozaki, H. et al. (2001). Overexpression of CDC25B overrides radiation-induced G2-M arrest and results in increased apoptosis in esophageal cancer cells. *Cancer Res.* **61**, 3188-3193.

Morgan, D. O. (1997). Cyclin-dependent kinases: engines, clocks, and microprocessors. *Annu. Rev. Cell Dev. Biol.* **13**, 261-291.

Muslin, A. J. and Xing, H. (2000). 14-3-3 proteins: regulation of subcellular localization by molecular interference. *Cell. Signal.* **12**, 703-709.

Muslin, A. J., Tanner, J. W., Allen, P. M. and Shaw, A. S. (1996). Interaction of 14-3-3 with signaling proteins is mediated by the recognition of phosphoserine. *Cell* **84**, 889-897.

Nagata, A., Igarashi, M., Jinno, S., Suto, K. and Okayama, H. (1991). An additional homolog of the fission yeast cdc25+ gene occurs in humans and is highly expressed in some cancer cells. *New Biol.* **3**, 959-968.

Nilsson, I. and Hoffmann, I. (2000). Cell cycle regulation by the Cdc25 phosphatase family. *Prog. Cell Cycle Res.* **4**, 107-114.

Nishi, K., Yoshida, M., Fujiwara, D., Nishikawa, M., Horinouchi, S. and Beppu, T. (1994). Leptomycin B targets a regulatory cascade of crm1, a fission yeast nuclear protein, involved in control of higher order chromosome structure and gene expression. *J. Biol. Chem.* **269**, 6320-6324.

O'Neill, T., Giarratani, L., Chen, P., Iyer, L., Lee, C. H., Bobiak, M., Kanai, F., Zhou, B. B., Chung, J. H. and Rathbun, G. A. (2002). Determination of substrate motifs for human Chk1 and hCds1/Chk2 by the oriented peptide library approach. *J. Biol. Chem.* **277**, 16102-16115.

Peng, C. Y., Graves, P. R., Thoma, R. S., Wu, Z., Shaw, A. S. and Piwnica-Worms, H. (1997). Mitotic and G2 checkpoint control: regulation of 14-3-3 protein binding by phosphorylation of Cdc25C on serine-216. *Science* **277**, 1501-1505.

Peng, C. Y., Graves, P. R., Ogg, S., Thoma, R. S., Byrnes, M. J. 3rd, Wu, Z., Stephenson, M. T. and Piwnica-Worms, H. (1998). C-TAK1 protein kinase phosphorylates human Cdc25C on serine 216 and promotes 14-3-3 protein binding. *Cell Growth Differ.* **9**, 197-208.

Rittinger, K., Budman, J., Xu, J., Volinia, S., Cantley, L. C., Smerdon, S. J., Gamblin, S. J. and Yaffe, M. B. (1999). Structural analysis of 14-3-3 phosphopeptide complexes identifies a dual role for the nuclear export signal of 14-3-3 in ligand binding. *Mol. Cell* **4**, 153-166.

Rothblum-Oviatt, C. J., Ryan, C. E. and Piwnica-Worms, H. (2001). 14-3-3 binding regulates catalytic activity of human Wee1 kinase. *Cell Growth Differ.* **12**, 581-589.

Sanchez, Y., Wong, C., Thoma, R. S., Richman, R., Wu, Z., Piwnica-Worms, H. and Elledge, S. J. (1997). Conservation of the Chk1 checkpoint pathway in mammals: linkage of DNA damage to Cdk regulation through Cdc25. *Science* **277**, 1497-1501.

Sebastian, B., Kakizuka, A. and Hunter, T. (1993). Cdc25M2 activation of cyclin-dependent kinases by dephosphorylation of threonine-14 and tyrosine-15. *Proc. Natl. Acad. Sci. USA* **90**, 3521-3524.

Tzivion, G., Shen, Y. H. and Zhu, J. (2001). 14-3-3 proteins; bringing new definitions to scaffolding. *Oncogene* **20**, 6331-6338.

Wang, Y., Jacobs, C., Hook, K. E., Duan, H., Booher, R. N. and Sun, Y. (2000). Binding of 14-3-3beta to the carboxyl terminus of Wee1 increases Wee1 stability, kinase activity, and G2-M cell population. *Cell Growth Differ.* **11**, 211-219.

Wang, X., Arooz, T., Siu, W. Y., Chiu, C. H., Lau, A., Yamashita, K. and Poon, R. Y. (2001). MDM2 and MDMX can interact differently with ARF and members of the p53 family. *FEBS Lett.* **490**, 202-208.

Yaffe, M. B. (2002). How do 14-3-3 proteins work? Gatekeeper phosphorylation and the molecular anvil hypothesis. *FEBS Lett.* **513**, 53-57.

Yaffe, M. B., Rittinger, K., Volinia, S., Caron, P. R., Aitken, A., Leffers, H., Gamblin, S. J., Smerdon, S. J. and Cantley, L. C. (1997). The structural basis for 14-3-3: phosphopeptide binding specificity. *Cell* **91**, 961-971.

Yang, J., Winkler, K., Yoshida, M. and Kornbluth, S. (1999). Maintenance of G2 arrest in the Xenopus oocyte: a role for 14-3-3-mediated inhibition of Cdc25 nuclear import. *EMBO J.* **18**, 2174-2183.

Yao, Y., Slosberg, E. D., Wang, L., Hibshoosh, H., Zhang, Y. J., Xing, W. Q., Santella, R. M. and Weinstein, I. B. (1999). Increased susceptibility to carcinogen-induced mammary tumors in MMTV-Cdc25B transgenic mice. *Oncogene* **18**, 5159-5166.

Continuous treatment of bestatin induces anti-angiogenic property in endothelial cells

Yuji Mishima,[1,2] Yasuhito Terui,[1,2] Natsuhiko Sugimura,[2] Yuko Matsumoto-Mishima,[1] Akiko Rokudai,[1] Ryoko Kuniyoshi[1] and Kiyohiko Hatake[1,2,3]

[1]Cancer Chemotherapy Center, Clinical Chemotherapy, Japanese Foundation for Cancer Research; [2]OLYMPUS Bio-Imaging Laboratory, Japanese Foundation for Cancer Research, 3-10-6, Ariake, Koto-ku, Tokyo, 135-8550, Japan

(Received July 12, 2006/Revised October 31, 2006/Accepted November 9, 2006/Online publication January 19, 2007)

CD13/aminopeptidase-N (CD13/APN) is an important regulator of angiogenesis where its expression on activated blood vessels is induced by angiogenic signals. A previous study demonstrated that angiogenesis is suppressed under the presence of high concentrations of aminopeptidase antagonists. However, the mechanisms underlying the inhibition of morphogenesis by aminopeptidase antagonists have not been elucidated. In this study, we have for the first time examined the effects of continuous treatment of therapeutic dose of aminopeptidase antagonists on vascular endothelial capillary-like tube formation. In the antagonists tested, only bestatin significantly interfered in the capillary tube formation of primary endothelial cells (EC) after treatment for 72 h. Aminopeptidase analysis revealed that inhibitory activity of bestatin was not specific for CD13/APN, and the other inhibitors lacking anti-angiogenic properties also inhibit cell-surface aminopeptidase activity as well or more potently than bestatin, suggesting that the angiogenesis-inhibitory effect of bestatin was not due to inhibition of CD13/APN activity at this concentration. To elucidate the influence of continuous treatment of bestatin on endothelial cells, we performed microarray analysis and revealed that 72-h treatment of a pharmacokinetic dose of bestatin modulated the several angiogenesis-related genes including *vascular endothelial growth factor* (*VEGF*). Northern blot analysis indicated that modulation of the *VEGF* gene became obvious after 48 h of treatment. Furthermore, knockdown of the *VEGF* gene by siRNA remarkably suppressed capillary tube formation and required a higher concentration of exogenous VEGF to reverse the capillary formation ability. These data suggested that bestatin decreases a reactivity of EC to angiogenesis stimuli, and it can be achieved by the regulation of angiogenesis-related gene expression. (*Cancer Sci* 2007; 98: 364–372)

Angiogenesis is the development of new blood vessels from pre-existing vasculature to provide a nutritive blood supply and is indispensable for tumor growth and survival.[1,2] The anti-angiogenic approach to antitumor treatment is thought not only to eradicate primary tumor tissues, but also to suppress tumor metastases.[3,4] In addition, because angiogenesis occurs at extremely low levels in the non-tumor-bearing adult organism, anti-angiogenic therapy is thought to be free of the severe side-effects that are usually seen with cytotoxic anticancer drugs.[5] Recent studies indicated that CD13/aminopeptidase-N (CD13/APN) cell-surface antigen expresses on endothelial cells (EC) of angiogenic vasculature but not normal ones.[6,7] Furthermore, aminopeptidase antagonists specifically inhibited chorioallantoic membrane angiogenesis and xenograft tumor growth.[8] Bhagwat *et al.* reported that CD13/APN in EC is activated by angiogenic signals and is essential for capillary tube formation.[6] They demonstrated that CD13/APN inhibitors effectively abrogate the ability of the cells to organize capillary formation. These effects are apparent at extremely high concentrations of CD13/APN inhibitors (>250 μM), and are thought to result from inhibition of aminopeptidase activity.

Previously, we have demonstrated that one of the CD13/APN inhibitors bestatin induces expression of *interleukin-8* (*IL-8*) mRNA.[9] Endothelial cell-derived interleukin (IL)-8 protein is different along with monocyte-derived IL-8 in primary structure, and the former induces apoptosis in leukemic cells, but the latter does not.[10–12] Ours was the first report stating that an aminopeptidase inhibitor modulates the expression of an antitumor molecule. The induction of *IL-8* gene expression was observed after 48 h of incubation with bestatin at a concentration within the pharmacokinetic dose (<10 μM). As mentioned above, aminopeptidase antagonists inhibit angiogenesis at extremely high doses, but the influence of continued exposure to aminopeptidase antagonists at a moderate dose has not been elucidated. The purpose of the current study is to clarify the effect of chronic treatment of APN antagonists on angiogenic potency and the regulation of gene expression of vascular EC.

Materials and methods

Reagents. Bestatin was provided by Nippon Kayaku (Tokyo, Japan). All other peptidase inhibitors were purchased from Sigma (St Louis, MO, USA). A monoclonal antibody that neutralizes CD13/APN, WM-15 and an isotype-matched control antibody (DD7) were purchased from Chemicon (Temecula, CA, USA). Matrigel was purchased from Collaborative Research (Waltham, MA, USA).

Cell and cell culture. Human umbilical vascular endothelial cells (HUVEC) and neonatal dermal microvascular endothelial cells (HMVEC) were purchased from Cambrex Bio Science (Walkersville, MD, USA), and were used from passages 2–7. Both HUVEC and HMVEC used in the present study were derived from pooled donors. Cells were routinely cultured in EGM-2 medium or EGM-2 MV medium, respectively, containing endothelial growth supplement according to the manufacturer's recommendations (Cambrex Bio Science). Neonatal human dermal fibroblasts (NHDF) were purchased form Cambrex Bio Science, and were cultured in FGM-2 medium (Cambrex Bio Science).

Aminopeptidase activity. Aminopeptidase activity was measured regarding the whole living cell and a cell surface and cytoplasm fraction of EC in triplicate experiments using different batches of HUVEC. For total aminopeptidase activity, HUVEC were suspended in phosphate-buffered saline (PBS, pH 7.4) at 1×10^5 cells/mL, and 100-μL aliquot was mixed with an equal volume of 200 μM alanine-(7-amino-4-methylcoumarine)acetic acid (Ala-MCA), leucine-MCA (Leu-MCA), methionie-MCA (Met-MCA), phenylalanine-MCA (Phe-MCA), lysine-MCA (Lys-MCA) or arginine-MCA (Arg-MCA) in a 96-well microtiter plate in the presence or absence of aminopeptidase inhibitors (final concentration of 10 μM) or WM-15 (final concentration of 10 μg/mL). Progress of fluorescent product (7-amino-4-methylcoumarine)

[3]To whom correspondence should be addressed. E-mail: khatake@jfcr.or.jp

doi: 10.1111/j.1349-7006.2007.00393.x
© 2007 Japanese Cancer Association

formation was recorded using a fluorometric plate reader (Fluoroskan Ascent, Helsinki, Finland) on kinetic mode at 37°C with a 355-nm excitation filter and a 460-nm emission filter. For cell-surface and cytoplasmic aminopeptidase, 1×10^6 cells were resuspended in 1 mL of PBS containing 1.0 μg/mL of leupeptin, pepstatin, and aprotinin, then homogenized by ultrasonication and the lysate was centrifuged for 60 min at 125 000 *g* at 4°C. Supernatant was collected and diluted 10-fold with PBS (cytoplasmic fraction; 1×10^5 cells/mL equivalency). Precipitate was resuspended in 1 mL of PBS containing 1.0 μg/mL of leupeptin, pepstatin and aprotinin by ultrasonication and diluted 10-fold with PBS (cell-surface fraction; 1×10^5 cells/mL equivalency). The aminopeptidase activity was calculated from the fluorescence of a 7-amino-4-methylcoumarine standard.

Cell proliferation assay. To determine cell numbers, 1.0×10^4 cells/well were seeded into 96-well plate in EGM-2 medium. An APN inhibitor, bestatin, amastatin, arphamenine-B or actinonin at the concentration of 10 μM, or WM-15 at the concentration of 10 μg/mL, was added. For negative control, 100 μg/mL of trypsin inhibitor with 0.1% dimethylsulfoxide (DMSO) or 10 μg/mL of isotype-matched control antibody were added. Cultures were incubated for 72 h at 37°C in a humidified atmosphere of 95% air and 5% CO_2. Each condition was performed in quadruplicate. After 72 h, cell numbers were assessed using a Cell Counting Kit (Dojin Laboratories, Kumamoto, Japan) to count living cells by combining 2-(2-methoxy-4-nitrophenyl)-3-(4-nitrophenyl)-5-(2,4-disulfophenyl)-2H-tetrazolium (WST-8) and 1-methoxy-phenazine methosulfate (1-methoxy-PMS). Control experiments comparing cell enumeration by the colorimetric assay or by direct counting after trypsinization showed an exact proportionality of data.

Capillary tube formation assay. HUVEC were cultured in the presence or absence of a CD13/APN antagonist for 72 h. The antagonists used were bestatin, amastatin, arphamenine-B or actinonin at the concentration of 10 μM or WM-15 at the concentration of 10 μg/mL. For negative control, 100 μg/mL of trypsin inhibitor containing 0.1% DMSO or 10 μg/mL isotype-matched control antibody were added. After 72 h treatment, the cells were detached by gentle treatment with 2 mM ethylene diamine tetra acetate (EDTA), and immediately resuspended in Dulbecco's minimum essential medium (DMEM) supplemented with 2% fetal calf serum (FCS) at the concentration of 2×10^4 cells/mL, and were then plated at a density of 1×10^4 cells/well onto a 48-well plate coated with 100 μL/well of growth-factor-reduced Matrigel (Becton Dickinson, Bedford, MA, USA). The plates were incubated at 37°C in a humidified atmosphere of 95% air and 5% CO_2. Capillary tube formation was assessed after 22–24 h by counting the total number of capillary-like tubular structures of each well using an inverted microscope (IX-81; Olympus, Tokyo, Japan) fitted with a confocal laser-scanning unit (FV-1000; Olympus).[13] The assay was performed using three different batches of HUVEC from pooled donors.

For rescue experiments by exogenous vascular endothelial growth factor (VEGF), 10 ng/mL or 100 ng/mL of recombinant VEGF (R&D Systems, Minneapolis, MN, USA) was added to the medium of capillary tube formation experiments.

Three-dimensional co-culture of EC and fibroblasts. Three-dimensional co-culture of EC and fibroblasts was performed as previously described.[14] Briefly, HMVEC monolayers were cultured to 80% confluency in 24-well glass bottom plate and then overlaid with a 1-mm layer of acellular collagen type I (2 mg/mL) prepared in M199 medium supplemented with heparin (100 U/mL), vitamin C (50 μg/mL) and FCS (10%). After polymerization, the cells were overlaid with a second (3 mm) collagen layer containing 4×10^5/mL NHDF (2.0×10^5 total cells). The endothelial cell growth medium (without endothelial growth supplement) was changed every 48 h. Experimental controls with only acellular collagen were constructed with the same sequence. To make a sharp distinction between EC and fibroblasts, HMVEC and NHDF were stained with PKH-2 (green fluorescence; Sigma) and PKH-26 (red fluorescence), respectively, before seeding. After 7 days, the three-dimensional morphology of the EC was observed by using confocal microscopy (FV-1000; Olympus). Observation was carried out at the position of the surface of culture matrix of the glass bottom plate and 200 μm above the surface of culture matrix, where endothelial cell and fibroblast had co-localized. The assay was performed using two different batches of HMVEC and NHDF combination. To confirm whether secretion of cytokines by fibroblast is affected by bestatin, the levels of VEGF, platelet-derived growth factor (PDGF)-BB, and basic-fibroblast growth factor (bFGF), which were representative angiogenic factors secreted by fibroblast was measured. NHDF was cultured alone with or without the presence of 10 μM aminopeptidase inhibitors for 7 days with a half-medium change on days 3 and 6 with added inhibitors. Conditioned media was collected after the third day and the sixth day from inhibitor addition, and assay was performed using commercially available ELISA kits (Quantikine, R&D Systems) according to the manufacturer's instructions. Additionally, total RNA was extracted at day 7, and semiquantitative reverse transcription polymerase chain reaction (RT-PCR) was performed using specific primers for $VEGF_{165}$, PDGF-β chain, and bFGF.

RNA isolation from HUVEC. HUVEC were treated with 10 μM bestatin, diluted from a 10 mM stock of DMSO or with an equivalent volume of DMSO (0.1%), for 72 h. The cells were then washed once with PBS and harvested with a cell-scraper. Total RNA from HUVEC was extracted by using an Atlas Glass Total RNA Isolation kit (Clontech), according to the manufacturer's instructions.

RNA quality assessment. Fifty nanograms of total RNA was assessed for quality by electrophoretic separation on a 2100 Bioanalyzer (Agilent Technologies). From the electopherogram, the quality of RNA was assessed by analysis of the 18S and 28S ribosomal subunit peak ratio. A 28S/18S peak ratio between 1.8 and 2.3 suggested RNA of high enough quality to proceed with microarray target labeling.

cDNA synthesis and fluorescent labeling. Labeled cDNA probes were synthesized from total RNA by using the Atlas Glass Fluorescent Labeling kit (Clontech). Briefly, 20 μg of total RNA was reverse transcribed with MMLV-Reverse Transcriptase using cDNA Synthesis (CDS) Primer (Clontech) that was designed to only synthesize cDNA for the genes printed on the array. During cDNA synthesis, primary aliphatic amino groups were incorporated using an optimized deoxyribonucleotide triphosphate (dNTP) mix, which includes the thymidine 5'-triphosphate (dTTP) analog, aminoallyl-deoxyuridine 5-triphosphate (dUTP). Synthesized cDNA were purified by ethanol precipitation, then resuspended in 10 μL of 2 × Atlas fluorescent labeling buffer (Clontech), mixed with 10 μL of 5 mM Cy3 monofunctional N-hydroxysuccinimide-activated dye (Amersham Pharmacia Biotech), and incubated in the dark at 25°C for 30 min. Labeled probes were purified by ethanol precipitation and Atlas NucleoSpin Extraction kit.

Microarray hybridization. An Atlas Glass Human 1.0 Microarray (Clontech), which contains DNA representing 1081 known genes, was used in these studies. The cDNA microarrays were hybridized with 21 mL of Atlas Glass Human Hybridization Solution in a Clontech Hyb Chamber (Clontech) at 50°C for 16 h. The arrays were washed with Clontech GlassHyb Wash Solution, ×1 standard saline citrate with one-tenth Clontech GlassHyb Wash Solution, and ×0.1 standard saline citrate each for 10 min at room temperature. The arrays were rinsed briefly with distilled water and dried, subsequently scanned fluorescent intensities with the GenePix-4000 A scanner (Axon Instruments).

© 2007 Japanese Cancer Association

Microarray data analysis. Data analysis was performed with AtlasImage Software 1.0 (Clontech). Expression values of transcripts were normalized to the total signal intensity on the membrane. The low signal threshold value was calculated by the gene-based signal threshold method. In agreement with the indications of the manufacturers, transcripts with a ratio of normalized expression levels of more than 2 or less than 0.5 were regarded as modulated.

Northern blot analysis. To assess the level of mRNA expression, northern blotting was performed as we previously described.[9] Briefly, total RNA from HUVEC was isolated with RNAzol B (Tel-Test, Friendswood, NJ, USA). Five micrograms of total RNA was fractionated by electrophoresis in formaldehyde/1.5% agarose gels, and bands were blotted onto a nitrocellulose membrane. RNA was cross-linked to membranes by ultraviolet (UV) irradiation (UV Strata-linker 1800; Stratagene, La Jolla, CA, USA). The membrane was hybridized first with a cDNA probe for the interested gene and then with a cDNA for *glyceraldehyde-3-phosphate dehydrogenase* (*G3PDH*), radiolabeled by use of a Random-Prime Labelling kit (Amersham Pharmacia, Piscataway, NJ, USA). Hybridization was performed at 68°C for 2 h, followed by stringent washing in 2.0–1.0–0.5–0.1 × standard saline citrate/0.1% sodium dodecyl sulfate (SDS) at 68°C for two 15-min periods. Hybridized membranes were exposed to Hyperfilm MP (Amersham Pharmacia) at −80°C.

Western blot analysis. To determine the alteration of cytoplasmic level of VEGF protein in EC exposed to aminopeptidase inhibitors, western blot analysis was carried out. HUVEC were seeded in six-well plates, treated with various aminopeptidase inhibitors, and harvested following the treatment. Cells were detached, harvested and lysed in a lysis buffer, containing 10 mM Tris-HCl (pH 6.8), 0.5% Triton, 5 mM EDTA and proteases inhibitors, for 30 min on ice. After removing the nuclei by centrifugation, 50 μg of protein from each sample was separated on 15–25% SDS–polyacrylamide gel electrophoresis (SDS-PAGE) and transferred onto a polyvinylidene difluoride (PVDF) membrane (Bio-Rad; Hercules, CA, USA) using standard techniques. Rabbit polyclonal antibodies against human VEGF (Santa Cruz, Santa Cruz, CA, USA) were used at a 1:200 dilution followed by a secondary antibody (horseradish peroxidase-conjugated goat antirabbit IgG; Santa Cruz) used at a 1:10 000 dilution. Antibody complexes were detected using the ECL system (Amersham). For negative control, 100 μg/mL of trypsin inhibitor with 0.1% DMSO was added.

siRNA transfection. HUVEC were transfected with either 20 nM control small interfering RNA (siRNA; Santa Cruz) or *VEGF* siRNA (Santa Cruz) using Lipofectamine RNAiMAX (Invitrogen), as described by the manufacturer. After a 48-h incubation in EGM-2 medium, cells were harvested and the silencing of *VEGF* gene and protein expression confirmed.

Results

Aminopeptidase activity of HUVEC treated with aminopeptidase antagonist. Recent report have indicated that CD13/APN in EC is activated by angiogenic signals.[6,7] HUVEC maintained in EGM-2 medium containing endothelial growth supplement such as VEGF or bFGF expresses a considerable amount of CD13/APN as well (data not shown). To evaluate the cell-surface aminopeptidase activity of HUVEC under the presence of various aminopeptidase antagonists, we performed the aminopeptidase assay using the fluorescence substrate, Ala-MCA, Leu-MCA, Met-MCA, Phe-MCA, Lys-MCA and Arg-MCA. Inhibitory activity of various chemical aminopeptidase antagonists and a CD13/APN neutralizing antibody, WM-15, was measured in living cells, cell membrane fraction and cytoplasmic fraction of HUVEC (Fig. 1a). As a result of the suppression experiment by WM-15, it was shown that aminopeptidase activity derived from CD13/APN accounted for approximately half of cell surface aminopeptidase activities, and the inhibitory activity of this antibody was not found in cytoplasm. Most aminopeptidase activity detected in living cells were collected in a cell membrane fraction, but high aminopeptidase activity, which could not be detected by living cell assay, was found in extracted cytoplasm. WM-15 was not able to inhibit cytoplasmic aminopeptidase, but the low-molecular aminopeptidase antagonists such as bestatin, amastatin, arphamenine-B and actinonin efficiently inhibited cytoplasmic aminopeptidase. Among these antagonists, amastatin and actinonin were effective to the peptidase activity for N-terminal neutral amino acid residues, and arphamenine-B preferentially inhibited aminopeptidase to a basic amino acid residue. In contrast, bestatin showed high inhibitory activity for hydrolysis of all examined N-terminal amino acid residue universally. To estimate the reversibility of aminopeptidase activity after the long term treatment by the antagonists, the aminopeptidase activity was measured in the cells that were treated with various inhibitors for 72 h and subsequently washed with PBS. Except for neutralization antibody WM-15, that strongly associates with a CD13/APN molecule, the aminopeptidase activity of HUVEC recovered to the same level as when activity measurements were carried out when there existed an antagonist at the concentration of 1:100 (Fig. 1b).

Effect of the chronic treatment of aminopeptidase inhibitors on proliferation of HUVEC. To assess the effect of aminopeptidase antagonists on proliferation of EC, we performed the cell proliferation assay in HUVEC treated with an aminopeptidase inhibitor, bestatin, amastatin, arphamenine-B, actinonin, or the CD13/APN neutralizing antibody, WM-15. The effect of aminopeptidase antagonists on HUVEC proliferation is shown in Figure 2. Actinonin significantly inhibited HUVEC proliferation after 3 days of incubation at the concentrations of 10 μM ($P < 0.05$). The inhibition was more dramatic at the concentrations of 50 μM ($P < 0.01$). However, other antagonists did not significantly affect HUVEC proliferation at concentrations as high as 10 μM (bestatin, amastatin and arphamenine-B) or 10 μg/mL (WM-15). The treatment with higher concentration (50 μM) slightly decreased the cell number, but a level of statistical significance was not attained. In the light of these results, APN antagonists except actinonin do not exhibit direct cytotoxicity to HUVEC.

Effect of the chronic treatment of aminopeptidase inhibitor on capillary tube formation of EC. Although it was reported that capillary tube formation of EC were suppressed under the presence of a high concentration of the aminopeptidase inhibitors, the effect of prolonged treatment of aminopeptidase antagonists at a moderate dose has not been elucidated.[6,15] To clarify the effect long-term treatment with an inhibitor of a moderate dosage, we performed a capillary tube formation assay by using the EC treated with 10 μM of an aminopeptidase inhibitor (bestatin, amastatin, arphamenine-B or actinonin) or 10 μg/mL of WM-15 for 72 h. To eliminate the effects of carry-over of antagonists, the cells were rinsed with PBS in order to flush the antagonist, then seeded on growth-factor-reduced Matrigel. As indicated in Figure 3(a), the total number of capillary-like tubular structures of the well was significantly reduced by the treatment of bestatin. Actinonin that has been shown the direct cytotoxicity to EC, slightly suppressed the capillary tube formation but a level of statistical significance was not attained. Although Matrigel tube formation assay is widely used for *in vitro* models of angiogenesis, and is a useful technique for quantification of angiogenic property, the molecular basis is still not completely elucidated. In order to further confirm the effect of aminopeptidase inhibitors on angiogenesis, we used an endothelium-fibroblast co-culture model that reflected EC detachment, invasion, migration, proliferation, and vacuole and tube formation. HMVEC was cultivated for 72 h in the medium containing the 10 μM of bestatin, amastatin, arphamenine-B, actinonin or 100 μg/mL of

doi: 10.1111/j.1349-7006.2007.00393.x
© 2007 Japanese Cancer Association

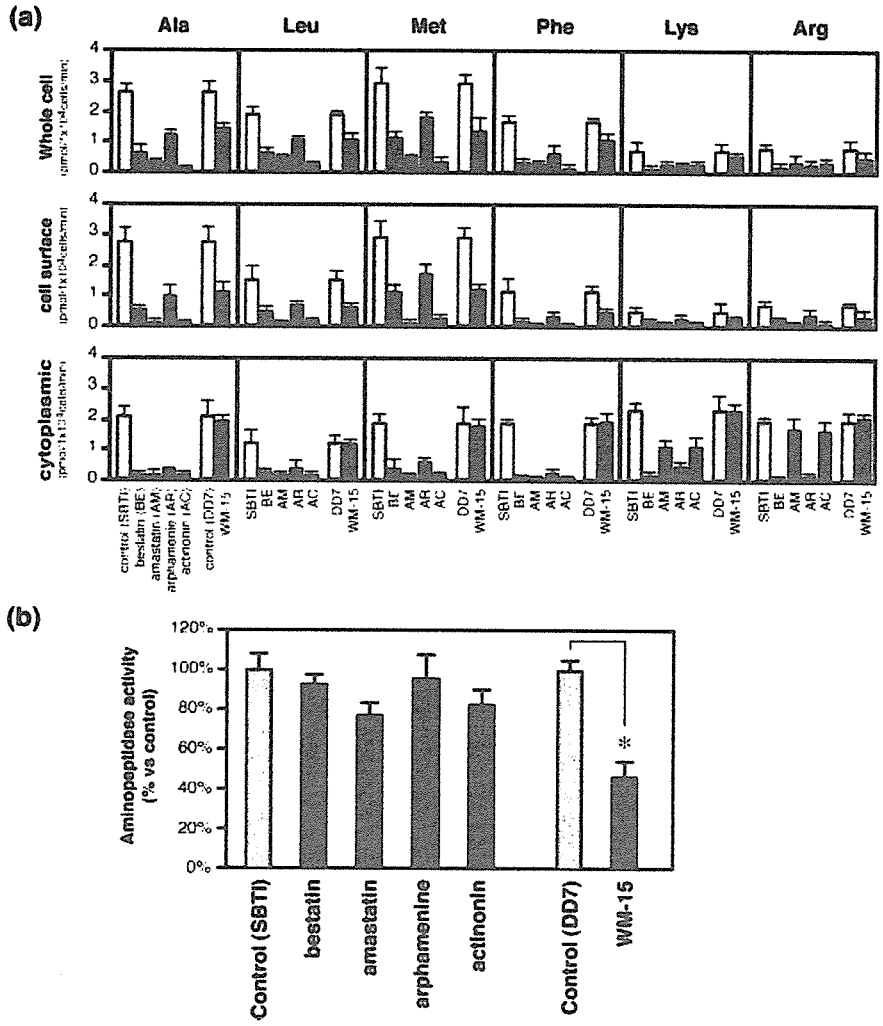

Fig. 1. Aminopeptidase activity was measured in the whole living cell, cell surface and cytoplasm fraction of endothelial cells (EC) using various antagonist-treated human umbilical vascular endothelial cells (HUVEC). (a) The aminopeptidase-activity of HUVEC was measured in the presence of 10 μM of aminopeptidase inhibitors (bestatin, amastatin, arphamenine-B or actinonin) or 10 μg/mL of a neutralizing antibody, WM-15. The aminopeptidase inhibitors were added directly to the aminopeptidase assay system and pre-incubated at 37°C for 30 min before addition of substrate. For the control experiments, soybean trypsin inhibitor (SBTI) or isotype matched immunoglobulin (Ig)G (DD7) were used. (b) Effects of 72-h treatment of aminopeptidase antagonists on aminopeptidase activity of living HUVEC. The cells were treated with aminopeptidase inhibitors (10 μM of bestatin, amastatin, arphamenine-B or actinonin) or a neutralizing antibody, WM-15 (10 μg/mL), for 72 h. After washing the cells with phosphate-buffered saline (PBS), the activity of aminopeptidase was measured. While WM-15 significantly suppressed the aminopeptidase activity of HUVEC even after washing, the inhibition of the other chemical inhibitor was almost reversible. Data are expressed as mean ± 95% confidence interval of the mean from three experiments; $*P < 0.01$ vs control.

soybean trypsin inhibitor (SBTI) with 0.1% DMSO (for control), then used for three-dimensional tube-formation assay, keeping a concentration of inhibitor of 10 μM. In the control group, some EC migrated into the acellular collagen layer, regardless of whether fibroblasts were present in the upper collagen layer or not (data not shown). The EC migrated through the acellular collagen into the fibroblast-containing collagen layer. They assumed an elongated, tubular morphology with branching cytoplasm after 7 days co-culture (Fig. 3b, a–f). EC were observed proliferating in collagen I even 7 days after overlay. In the groups that added an inhibitor except bestatin, a remarkable difference was not observed in comparison with the control group (data not shown). On the other hand, in the group where bestatin was added, a considerable amount of EC were left on the matrix of the culture dish and a smaller number of EC migrated into the fibroblast-containing collagen layer; however, the proliferation and/or tubular formation of EC in the fibroblast layer were less apparent than observed in the control group (Fig. 3b, g–l).

To examine whether bestatin affected the angiogenesis-supporting ability of fibroblast, levels of pro-angiogenic cytokines in conditioned media and corresponding gene expression were analyzed in NHDF cultured alone with addition of aminopeptidase inhibitors. As shown in Figure 3(c), at least regarding VEGF and bFGF, 10 μM of bestatin treatment did not affect the secretion of pro-angiogenic cytokine from NHDF. Secretion of PDGF-BB was under detection levels, but expression levels of all these genes were revealed to be unchanged by bestatin addition. Also, bestatin addition did not affect the proliferation of NHDF significantly (data not shown).

Comprehensive gene expression analysis of bestatin-treated EC. One of the CD13/APN inhibitors, 72 h of moderate dose bestatin treatment suppresses capillary-like tubular formation, although a greater part of aminopeptidase activity remains. This result indicates that other mechanisms than aminopeptidase suppression may exist. To confirm this hypothesis, alteration of gene expression in vascular cells was analyzed by using the technique of cDNA microarray in order to characterize the effect of chronic treatment of bestatin.

The obtained fluorescent intensity data were background-corrected, and the signal intensity between the two arrays subsequently normalized. The calculated threshold value was 239. Figure 4a shows the differences in the gene expression pattern between control and bestatin-exposed HUVEC. Among the relevant 1081 genes assembled in the cDNA microarray, 19 were found to be modulated by treatment of bestatin, with a difference of signal intensity ratio of more than 2. Genes were divided into two groups on the basis of the difference in signal intensity: Out of 19 differentially expressed genes, eight were upregulated (signal intensity ratio >2) in bestatin-treated HUVEC compared with DMSO-treated control cells, and 11 were downregulated (signal intensity ratio <0.5). Results are shown in Table 1. Our comparative hybridization studies demonstrated that 72-h treatment with bestatin modulates many important angiogenesis-related genes in mRNA levels such as *VEGF*,

© 2007 Japanese Cancer Association

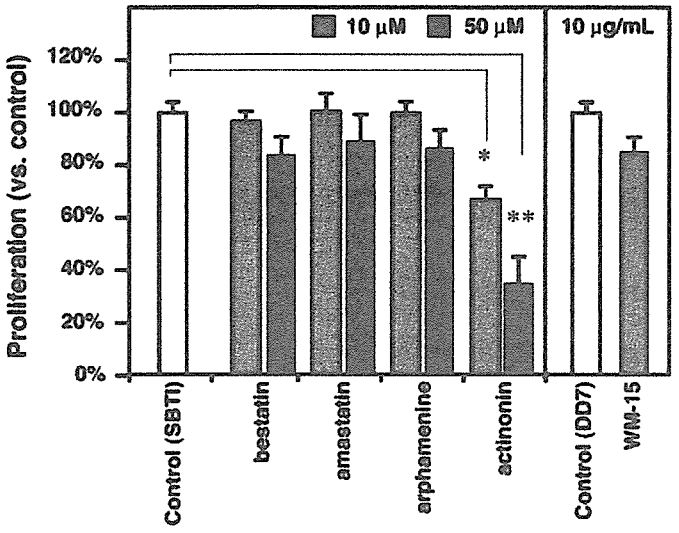

Fig. 2. Effects of 72-h treatment of aminopeptidase antagonists on the proliferation of EC. HUVEC was treated with bestatin, amastatin, arphamenine-B, actinonin (10 μM or 50 μM), and a neutralizing antibody, WM-15 (10 mg/mL), for 72 h, then viable cell numbers were determined, as described in Materials and Methods. For the control experiments, SBTI or isotype-matched IgG (DD7) were used. Data are expressed as percentages for control cell number. Error bars, 95% confidence interval of the mean. $*P < 0.05$, $**P < 0.01$ vs control.

Table 1. The differentially expressed genes

Gene	Ratio†
Upregulated gene	
CD71 antigen	3.77
nuclear factor NF90	3.22
colorectal cancer suppressor protein	2.08
jagged homologue 2	2.06
43-kDa postsynaptic protein	2.06
tissue inhibitor of metalloproteinase 1	2.04
Na^+/K^+-transporting ATPase isoform 2 beta polypeptide 2	2.04
collagen VI alpha subunit	2.01
Downregulated gene	
bone morphogenetic protein 2A	0.07
bone morphogenetic protein 1	0.15
transforming growth factor alpha	0.22
platelet-derived growth factor B subunit	0.27
bone morphogenetic protein 8	0.28
pancreatitis-associated protein 1	0.34
hepatocyte growth factor activator	0.35
CD4 antigen	0.38
vascular endothelial growth factor	0.46
cardiac muscle sodium channel alpha subunit	0.47
oncostatin M	0.47

†Ratio of intensity of fluorescence of bestatin-treated group for control group

PDGF-β, tissue inhibitor of metalloproteinase 1 (*TIMP-1*) and *bone morphogenetic protein* (*BMP*). Previously, we demonstrated that expression of the *IL-8* gene is upregulated by bestatin treatment. In the present study, the DNA microarray data suggests that the expression of the *IL-8* gene increased by 2.8-fold in the bestatin-treated group, but it was omitted because the signal intensity was less than the threshold value.

Northern blot analysis. To establish the validity of the microarray data, we analyzed the patterns of expression of some groups of genes by northern blot analysis, using the RNA extracted from the HUVEC treated with various time period or dosage of bestatin (Fig. 4b). The *VEGF* gene contains eight exons.[16] Analysis of *VEGF* cDNA predicts three major alternately spliced VEGF protein isoforms: $VEGF_{121}$ (lacking exons 6 and 7), $VEGF_{165}$ (lacking exon 6) and $VEGF_{189}$. Northern blot analysis revealed that $VEGF_{189}$ (5.2 kb) and $VEGF_{165}$ (4.5 kb) were downregulated by the dose- and time-dependent treatment of bestatin. The band at 3.7 kb corresponding to $VEGF_{121}$ was faint and inconstantly visible (data not shown). These changes of mRNA expression were prominent after 24 h of treatment. The gene expression of the major receptors for VEGF (*Flt-1* nor *KDR*) was not changed by bestatin treatment in agreement with the results of the microarray analysis. The *PDGF-β* subunit was downregulated by dose-dependent bestatin treatment, whereas the *PDGF-α* subunit was not. Besides the endothelial growth factors, gene expression of *matrix metalloproteinases (MMP)-1* was downregulated by dose-dependent bestatin treatment. The down-modulation was remarkable after 48 h treatment. On the other hand, the expression of *TIMP-1*, one of the inhibitory proteins of MMP, was upregulated. The increase in *TIMP-1* mRNA expression had reached a plateau at a relatively low dose of bestatin treatment (>2 μM), and it was prominent after 48 h.

Western blot analysis. To confirm the protein expression of VEGF, PDGF-β subunit and TIMP-1, western blotting and ELISA were performed on cell lysate and conditioned medium of APN-inhibitor-treated HUVEC. The protein of PDGF-β subunit and TIMP-1 were under the detectable level in both cell lysate and conditioned medium (data not shown). VEGF protein also could not be detected in the conditioned medium, using enzyme-linked immunosorbent assay (ELISA) and western blot analysis. The cytoplasmic VEGF protein expression was decreased by treatment with bestatin and actinonin after 3 days (Fig. 4c). Among the subtypes of VEGF, $VEGF_{165}$ was dominant and $VEGF_{121}$ and $VEGF_{189}$ were not detected. The suppression level by bestatin was prominent in comparison with that of actinonin.

VEGF silencing is associated with the attenuation of tube formation ability. To confirm the downregulation of cytoplasmic VEGF protein is associated with the attenuation of the capillary tube formation of EC, we established conditions for siRNA oligonucleotide-based depletion of VEGF. A liposome-based transfection of 20 nM siRNA for VEGF resulted in the downregulation of cytoplasmic VEGF to the same extent as that of bestatin treatment (Fig. 5a,b). By the quantification study of Matrigel tube formation, we confirmed that capillary tube formation was significantly decreased in the VEGF-silenced EC (Fig. 5c). We further examined whether bestatin-induced abrogation of tube-like formation in Matrigel is rescued by addition of VEGF or not. Matrigel capillary tube formation assay was performed using bestatin-treated HUVEC and VEGF-knockdown cells by siRNA with or without addition of 10 or 100 ng/mL of recombinant VEGF. Bestatin treatment was conducted at 10 μM for 3 days. Addition of exogenous VEGF rescued the suppression of tube formation in both bestatin-treated HUVEC and VEGF-siRNA-transfected HUVEC in a dose-dependent manner. In contrast, in non-treated HUVEC as well as control siRNA-transfected cells, capillary structure became more compact by addition of recombinant VEGF (data not shown).

Discussion

Accumulating evidences indicate that progressive tumor growth is dependent on angiogenesis.[17–19] Cancers cannot grow beyond a few cubic millimeters in volume unless they have their own blood supply.[1] On the other hand, in normal tissue, new blood vessels are formed in response to signals generated during tissue growth and repair (wound healing), during the normal female reproductive cycle, and during the development of the fetus in

doi: 10.1111/j.1349-7006.2007.00393.x
© 2007 Japanese Cancer Association

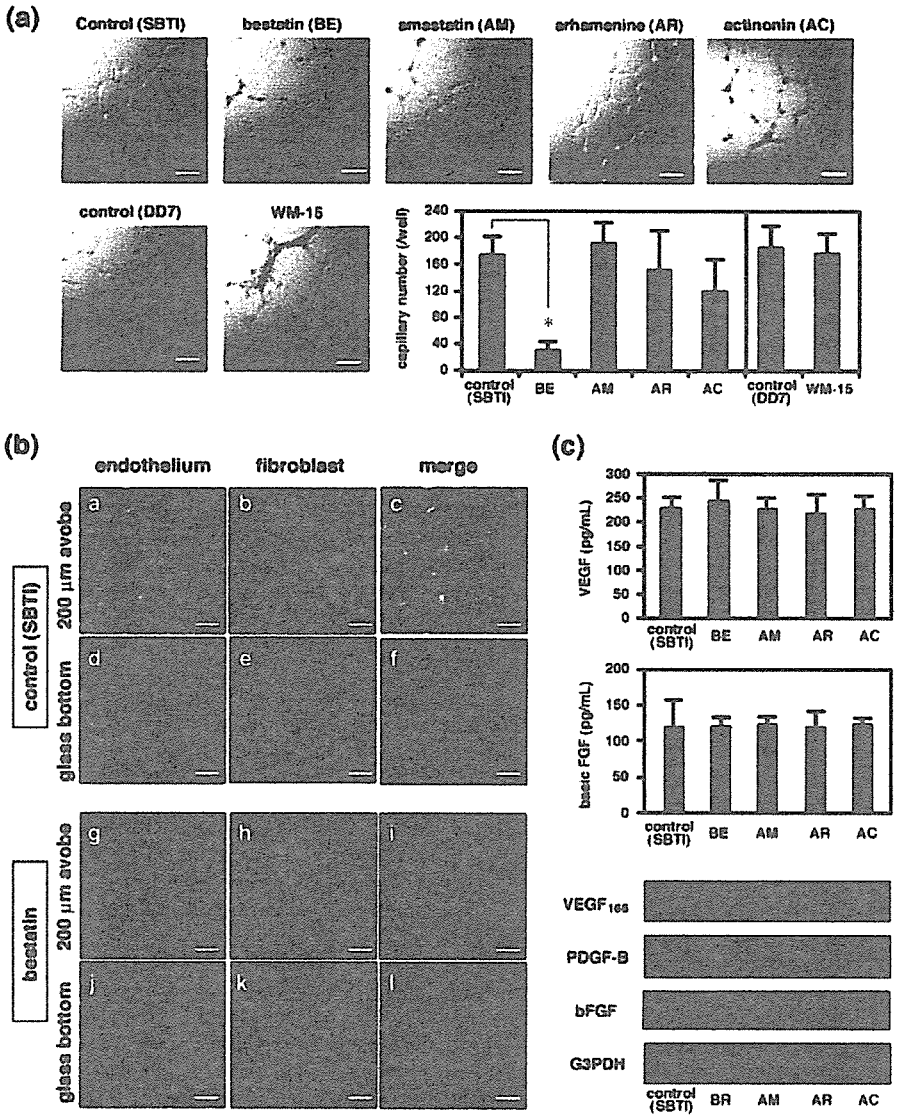

Fig. 3. Effects of 72-h treatment of aminopeptidase antagonists on the capillary tube formation of EC. (a) Matrigel capillary tube-like network formation assay. HUVEC was treated with bestatin, amastatin, arphamenine-B, actinonin (10 μM), and a neutralizing antibody, WM-15 (10 μg/mL), for 72 h, and cultured on a growth-factor-reduced Matrigel-coated plate for 22–24 h at 37°C. For the control experiments, SBTI or isotype-matched IgG (DD7) were used. The images were captured with a confocal microscope and the capillary-like tubular structure of each well was counted under the light microscope. The capillary tube formation of cells treated with bestatin were significantly suppressed. Representative of three independent experiments using different batches of HUVEC. Bar, 200 μm. Data are expressed as mean ± 95% confidence interval of the mean from three experiments. $^*P < 0.01$ vs control. (b) Three-dimensional co-culture of EC and fibroblasts. A neonatal dermal microvascular endothelial cells (HMVEC) monolayer was cultured to 80% confluency, overlaid with collagen I, followed by a second overlay of collagen I with neonatal human dermal fibroblasts (NHDF). After incubation for 7 days, the three-dimensional morphology of the EC was observed by confocal microscopy. Observation was carried out at the position of the surface of culture matrix of glass bottom plate and 200 μm above the surface of culture matrix, where endothelial cells and fibroblast co-localized. (a,d,g,l) HMVEC stained with PKH-2. (b,e,h,k) NHDF stained with PKH-26. (c,f,i,l) Merged image. (a–f) Control experiment added SBTI and dimethylsulfoxide (DMSO). (g–i) HMVEC was cultivated for 72 h in the medium containing the 10 μM of bestatin, and bestatin concentration kept at 10 μM during the co-culture. The tube-like network-morphology of EC was observed at the position of 200 μm above the surface of culture matrix in the control group (a–f). However, fewer EC migrated into the acellular collagen layer and tubular formation of EC were less apparent in the bestatin-treated group on day 7 (g–h). Representative of two independent experiments using different batches of HMVEC and NHDF combination. Bar, 200 μm. (c) To eliminate the effect of bestatin on angiogenesis-supporting ability of fibroblast, levels of vascular endothelial growth factor (VEGF), platelet derived growth factor (PDGF)-BB and basic fibroblast growth factor (FGF) in conditioned media and corresponding gene expression were analyzed in fibroblast cultured alone with addition of aminopeptidase inhibitors. Upper panels show the results of VEGF and bFGF concentration in conditioned media. The concentration of PDGF-BB was under detectable level (data not shown). Lower panels show the electrophoresis image of reverse transcription polymerase chain reaction (RT-PCR) product of *VEGF* (28 cycle amplification), *PDGF-BB* (38 cycles), *basic FGF* (28 cycles) and housekeeping gene, *glyceraldehyde-3-phosphate dehydrogenase* (*G3PDH*; 28 cycles).

pregnancy.[20] To date, several proteins have been identified to activate new blood vessel growth. Among these, the most potent is thought to be VEGF.[21] Besides VEGF, it has been confirmed that quite a few factors such as bFGF, angiogenin, epidermal growth factor (EGF), placental growth factor (PlGF), PDGF and tumor necrosis factor alpha (TNF-α) participate in angiogenesis.[22,23] In tumor tissue, tumor cells produce VEGF and other factors, which induce the existing blood vessels to make new blood vessels for the growth of the tumor in the surrounding tumor environment.[21]

© 2007 Japanese Cancer Association

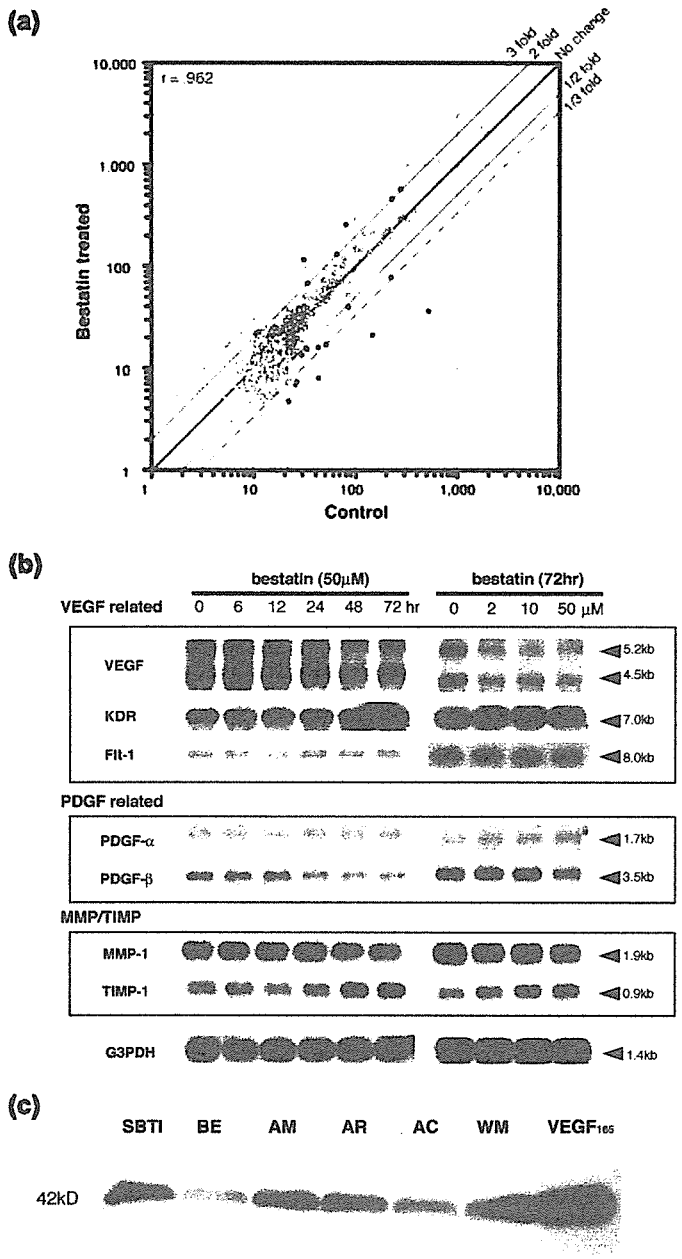

Fig. 4. Comprehensive gene expression analysis of bestatin-treated EC. (a) Scatter plot of normalized intensities (log scale) for gene expression of bestatin-treated HUVEC vs that of control cells. Nineteen genes were found to be modulated by 72 h of bestatin treatment (●). The gene of a fluorescent intensity less than 239, either the bestatin-treated or control cells, were omitted in order to avoid false positive (○). (b) Northern blot analysis of HUVEC with probes of angiogenic related genes. HUVEC was treated with 50 μM bestatin for 0–72 h (left) or 0–50 μM for 72 h (right) and total RNA was isolated. Northern blot hybridization was performed with the probe indicated. *G3PDH* probe was used for normalization of expression levels in the different lanes. (c) Western blot analysis of VEGF in HUVEC treated with an aminopeptidase antagonist for 72 h. A polyclonal antibody that could recognize three major isoforms was used. In HUVEC, VEGF165 was dominant and VEGF121 and VEGF189 were not detected. The cytoplasmic VEGF protein expression was decreased by treatment with bestatin and actinonin after 3 days. BE, bestatin; AM, amastatin; AR, arphamenine-B; AC, actinonin; WM, WM-15; VEGF165, recombinant VEGF165 control.

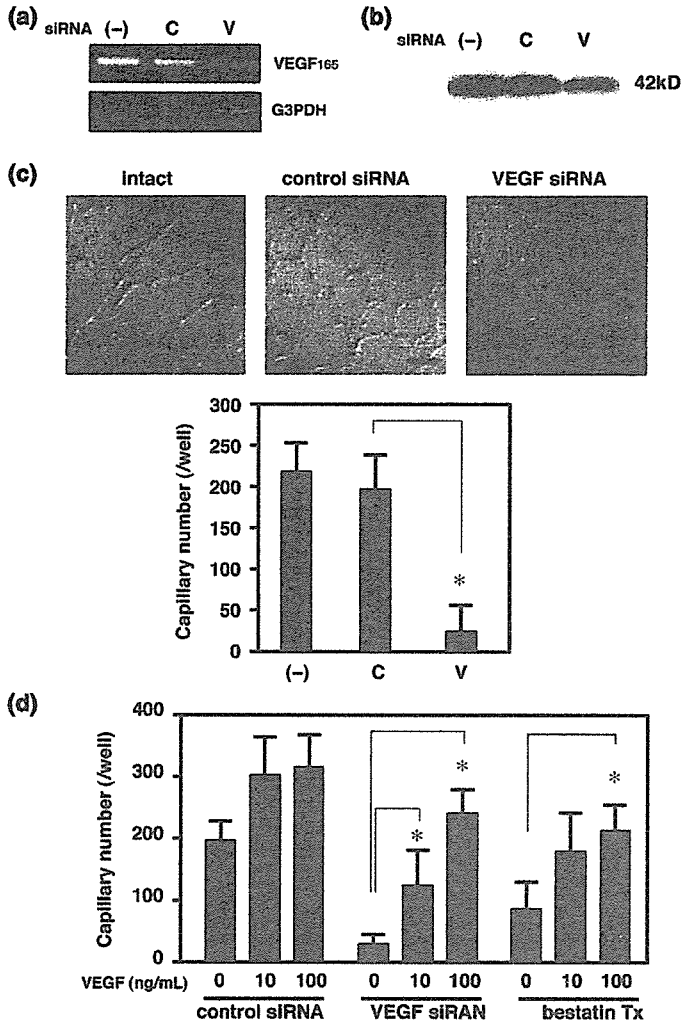

Fig. 5. VEGF silencing is associated with the attenuation of tube formation ability. (a) VEGF siRNA silenced $VEGF_{165}$ mRNA as determined by semiquantitative RT-PCR. (b) Gene silencing of *VEGF* resulted in the downregulation of cytoplasmic VEGF protein level as determined by Western blot. (c) Matrigel capillary tube-like network formation assay revealed VEGF silencing significantly decreased the capillary tube formation of EC. Representative of three independent experiments using different batches of HUVEC. Bar, 200 μm. Data are expressed as mean ± 95% confidence interval of the mean from three experiments. *$P < 0.01$ vs siRNA control. (–), intact HUVEC; C, control siRNA; V, VEGF siRNA. (d) Exogenous VEGF rescues the inhibition of capillary tube formation. Matrigel capillary tube formation assay was performed using bestatin-treated HUVEC and VEGF knockdown cells by siRNA with or without addition of 10 or 100 ng/mL of recombinant VEGF. Addition of exogenous VEGF rescued the suppression of tube formation in both bestatin and VEGF-siRNA treated HUVEC in a dose-dependent manner.

Endothelial cells, that compose the walls of blood vessels, play particularly important roles during angiogenesis. Responding to these signals from tumor cells, EC proliferate, destroying their surrounding tissue barriers with MMP enzymes, and migrate toward the tumor to form a connection to the blood supply.[24,25] Thus, the activation of EC is the key phenomenon of tumor angiogenesis. Recently, several studies have demonstrated that CD13/APN is an important regulator of angiogenesis where its expression on activated blood vessels is induced by angiogenic signals. However, the relationship between activation and CD13/APN induction have not been elucidated. Although previous studies have demonstrated that aminopeptidase inhibitor or

doi: 10.1111/j.1349-7006.2007.00393.x
© 2007 Japanese Cancer Association

CD13/APN-neutralizing antibody abrogate the ability of the EC to organize a capillary network, the doses of antagonists necessary for inhibiting tube-formation are extremely high (>250 μM) as compared with pharmacokinetic blood concentration of bestatin, the representative drug medicine of the APN/CD13 antagonists.[6,15] Indeed, bestatin did not interfere with capillary tube formation at a transiently-added concentration of less than therapeutic blood level (<10 μM; data not shown). In our previous study, we demonstrated that 48-h treatment of pharmacokinetic dose of bestatin to the CD13/APN-expressing leukemia cell reverses the resistance to apoptosis induction, accompanied by induction of the mRNA of an apoptosis-inducing peptide.[9] Thus, continuous treatment of CD13/APN antagonists might have distinct effects on the CD13/APN-expressing cells. To address this hypothesis, we investigated the effect of 72-h treatment of CD13/APN antagonists on the angiogenic activity of primary EC. Seventy-two hours of treatment of 10 μM of aminopeptidase antagonist, except actinonin, had no significant effect on the proliferation of HUVEC. Treatment of actinonin suppresses the proliferation of HUVEC to 68% of control, and induced apoptosis in a part of the cells (data not shown). In the treatment with the higher dose (50 μM), the cytotoxicity of actinonin was more prominent, and other chemical antagonists suppress the proliferation of HUVEC slightly, but these effects did not reach statistical significance. The capillary tube formation assay of the antagonist-pretreated cells revealed that only bestatin significantly abolishes the tube formation ability. Because the cell surface aminopeptidase activity of bestatin-treated cells was recovered to 90% of the control by washing out the residual bestatin, or because other inhibitors have no significant effect on capillary formation, it is unlikely that the inhibition of the aminopeptidase activity was solely responsible for the anti-angiogenic property of bestatin treatment. In order to clarify the mechanisms underlying the angiogenesis-suppressive effects of the continuous treatment of bestatin, we performed the gene expression analysis of the bestatin-treated primary EC. Treatment conditions were settled at the concentration of 10 μM of bestatin, or the equivalent concentration of DMSO, for 72 h. This concentration was chosen because the mean of maximum serum concentrations of bestatin after a single standard dose (30 mg/day) was determined to be 2.2 μg/mL (7.2 μM) and, after repeated administration, maximum serum concentrations of bestatin were slightly increased.[26] By analyzing the expression profile of the cDNA microarray containing 1101 known genes, eight genes were upregulated more than twofold while 11 genes were downregulated in the bestatin-treated EC when compared with the DMSO-treated control. Among these genes, *VEGF* and *PDGF-β* chain are included in the downregulated genes, and *TIMP-1*, an endogenous inhibitor of matrix metalloproteinase that degrades the extracellular matrix, is included in the upregulated genes.[27] In addition, several BMP (*BMP-1*, *BMP2A* and *BMP8*) were downregulated (to 15%, 7.0% and 28%, respectively). Among these, modulation of expression in the protein level was confirmed only in VEGF. The alteration of the protein expression of other molecules could not be analyzed because of low expression levels. VEGF is considered to be the most important angiogenic factor. In normal tissues, its receptors specifically express in the EC from the early stage of development, and intensive VEGF expression is observed at the angiogenic stages.[28] In the present study, we demonstrated that 72 h of bestatin treatment downregulates both mRNA and cytoplasmic protein expression of VEGF in EC. In addition, silencing of the VEGF gene by siRNA caused the cytoplasmic VEGF downregulation in the primary EC and decreased the capillary tube formation *in vitro*. Furthermore, we demonstrated that the exogenous addition of recombinant VEGF reversed the capillary formation ability of in both bestatin and VEGF-siRNA-treated HUVEC in a dose-dependent manner. The secretion of VEGF from tumor cells is an important trigger of the tumor angiogenesis. In addition, several studies demonstrated that activated EC secrete VEGF as well and induce their own VEGF mRNA expression.[29] Namely, VEGF operates not only in a paracrine manner but also in an autocrine manner. Bestatin treatment may block this autocrine loop, and this would suggest the explanation of the mechanism responsible for the anti-angiogenic effect of bestatin. This hypothesis may also explain the reason why bestatin suppressed the proliferation of EC only in the three-dimensional co-culture model. In the proliferation assay, because the medium was supplemented with the endothelial growth factors, such as VEGF, bFGF or insulin-like-growth factor, auto-activation was not required for survival or for the presence of excessive growth factors. On the other hand, growth factors were only derived from fibroblast in the three-dimensional co-culture model; hence, the autocrine loop of VEGF would be necessary for survival and proliferation of EC.

Downregulation of the gene and protein expression of VEGF was specific to bestatin, except for the actinonin. Treatment by actinonin showed a cytotoxic effect for endothelial cells, and decreased the protein level of VEGF, but the degree of downregulation was lower than bestatin. Because tendency to suppress the capillary tube formation was observed in actinonin-treated EC, degradation of VEGF-expression may also contribute to angiogenetic inhibition even in the case of actinonin.

The cell surface aminopeptidase activity including CD13/APN was inhibited by bestatin of pharmacokinetic concentration. However, the degree of suppression was not more potent than amastatin and actinonin that did not inhibit capillary tube formation. In addition, the inhibition by bestatin was reversible. These results suggest that inhibition of aminopeptidase activity of CD13/APN is not a direct mechanism of angiogenesis inhibition in continuous bestatin treatment. Recently, several aminopeptidases that are localized in cytoplasm of EC, such as puromycin insensitive leucyl-specific aminopeptidase (PILSAP) or methionine aminopeptidases type2 (MetAp2) have been suggested to play an important role in angiogenesis.[30–33] In addition, it has been reported that bestatin can be transported through peptide transporter-mediated processes in the cells of some organs such as liver, kidneys and intestine, and also indicated that bestatin inhibits cytosolic exopeptidases in mammalian reticulocytes, in the liver cytosol and in skeletal muscles.[34–36] In this study, although it was not able to clarify whether bestatin is uptaken in living EC or inhibits cytoplasmic aminopeptidase, bestatin showed broad inhibitory activity against the extracted cytosolic aminopeptidase that hydrolyze both neutral- and basic-amino acid residues. A possible explanation for anti-angiogenic modulation of bestatin is that continuous inhibition of some intracytoplasmic aminopeptidase may contribute to the regulation of the expression of angiogenesis-related molecules including VEGF.

Bestatin has been used clinically for years as an immunotherapy drug. Recently, a randomized phase III study of bestatin as a postoperative adjuvant treatment in patients with stage I squamous cell lung cancer was carried out, and statistically significant clinical improvement in overall survival and disease-free survival was ascertained.[37] However, the mechanisms of the antitumor effects of bestatin are not fully understood. The present study explains a portion of antitumor effects of bestatin as an adjuvant medicine. In addition, the angiogenesis-inhibitory effect of bestatin is an important clue that will help to elucidate the participation of aminopeptidases in the angiogenic process.

Acknowledgments

This work was supported in part by a Grant-in-Aid for Scientific Research on Priority Areas 'CANCER' from the Ministry of Education, Culture, Sports, Science, and Technology of Japan.

© 2007 Japanese Cancer Association

References

1 Folkman J. Angiogenesis in cancer, vascular, rheumatoid and other disease. *Nat Med* 1995; **1**: 27–31.
2 Yancopoulos GD, Davis S, Gale NW, Rudge JS, Wiegand SJ, Holash J. Vascular-specific growth factors and blood vessel formation. *Nature* 2000; **407**: 242–8.
3 Peyruchaud O, Serre CM, NicAmhlaoibh R, Fournier P, Clezardin P. Angiostatin inhibits bone metastasis formation in nude mice through a direct anti-osteoclastic activity. *J Biol Chem* 2003; **278**: 45 826–32.
4 Saaristo A, Karpanen T, Alitalo K. Mechanisms of angiogenesis and their use in the inhibition of tumor growth and metastasis. *Oncogene* 2000; **19**: 6122–9.
5 Folkman J. Seminars in Medicine of the Beth Israel Hospital, Boston. Clinical applications of research on angiogenesis. *N Engl J Med* 1995; **333**: 1757–63.
6 Bhagwat SV, Lahdenranta J, Giordano R, Arap W, Pasqualini R, Shapiro LH. CD13/APN is activated by angiogenic signals and is essential for capillary tube formation. *Blood* 2001; **97**: 652–9.
7 Curnis F, Arrigoni G, Sacchi A *et al.* Differential binding of drugs containing the NGR motif to CD13 isoforms in tumor vessels, epithelia, and myeloid cells. *Cancer Res* 2002; **62**: 867–74.
8 Pasqualini R, Koivunen E, Kain R *et al.* Aminopeptidase N is a receptor for tumor-homing peptides and a target for inhibiting angiogenesis. *Cancer Res* 2000; **60**: 722–7.
9 Mishima Y, Matsumoto-Mishima Y, Terui Y *et al.* Leukemic cell-surface CD13/aminopeptidase N and resistance to apoptosis mediated by endothelial cells. *J Natl Cancer Inst* 2002; **94**: 1020–8.
10 Terui Y, Tomizuka H, Mishima Y *et al.* NH2-terminal pentapeptide of endothelial interleukin 8 is responsible for the induction of apoptosis in leukemic cells and has an antitumor effect in vivo. *Cancer Res* 1999; **59**: 5651–5.
11 Terui Y, Ikeda M, Tomizuka H *et al.* Identification of a novel apoptosis-inducing factor derived from leukemic cells: endothelial interleukin-8, but not monocyte-derived, induces apoptosis in leukemic cells. *Biochem Biophys Res Commun* 1998; **243**: 407–11.
12 Terui Y, Ikeda M, Tomizuka H *et al.* Activated endothelial cells induce apoptosis in leukemic cells by endothelial interleukin-8. *Blood* 1998; **92**: 2672–80.
13 Pollman MJ, Naumovski L, Gibbons GH. Endothelial cell apoptosis in capillary network remodeling. *J Cell Physiol* 1999; **178**: 359–70.
14 Velazquez OC, Snyder R, Liu ZJ, Fairman RM, Herlyn M. Fibroblast-dependent differentiation of human microvascular endothelial cells into capillary-like 3-dimensional networks. *Faseb J* 2002; **16**: 1316–8.
15 Aozuka Y, Koizumi K, Saitoh Y, Ueda Y, Sakurai H, Saiki I. Anti-tumor angiogenesis effect of aminopeptidase inhibitor bestatin against B16-BL6 melanoma cells orthotopically implanted into syngeneic mice. *Cancer Lett* 2004; **216**: 35–42.
16 Tischer E, Mitchell R, Hartman T *et al.* The human gene for vascular endothelial growth factor. Multiple protein forms are encoded through alternative exon splicing. *J Biol Chem* 1991; **266**: 11 947–54.
17 Liao F, Li Y, O'Connor W *et al.* Monoclonal antibody to vascular endothelial-cadherin is a potent inhibitor of angiogenesis, tumor growth, and metastasis. *Cancer Res* 2000; **60**: 6805–10.
18 Willett CG, Boucher Y, di Tomaso E *et al.* Direct evidence that the VEGF-specific antibody bevacizumab has antivascular effects in human rectal cancer. *Nat Med* 2004; **10**: 145–7.
19 Rofstad EK, Halsor EF. Vascular endothelial growth factor, interleukin 8, platelet-derived endothelial cell growth factor, and basic fibroblast growth factor promote angiogenesis and metastasis in human melanoma xenografts. *Cancer Res* 2000; **60**: 4932–8.
20 Augustin HG, Braun K, Telemenakis I, Modlich U, Kuhn W. Ovarian angiogenesis. Phenotypic characterization of endothelial cells in a physiological model of blood vessel growth and regression. *Am J Pathol* 1995; **147**: 339–51.
21 Machein MR, Plate KH. Role of VEGF in developmental angiogenesis and in tumor angiogenesis in the brain. *Cancer Treat Res* 2004; **117**: 191–218.
22 Dobrescu G. The role of the endothelium in angiogenesis. *Rev Med Chir Soc Med Nat Iasi* 1997; **101**: 31–9.
23 Sun J, Wang DA, Jain RK *et al.* Inhibiting angiogenesis and tumorigenesis by a synthetic molecule that blocks binding of both VEGF and PDGF to their receptors. *Oncogene* 2005; **24**: 4701–9.
24 Arbiser JL, Moses MA, Fernandez CA *et al.* Oncogenic H-ras stimulates tumor angiogenesis by two distinct pathways. *Proc Natl Acad Sci USA* 1997; **94**: 861–6.
25 Nelson AR, Fingleton B, Rothenberg ML, Matrisian LM. Matrix metalloproteinases: biologic activity and clinical implications. *J Clin Oncol* 2000; **18**: 1135–49.
26 Ueda T, Tohyama K, Wano Y *et al.* Pharmacokinetic and clinical pilot study of high-dose intermittent ubenimex treatment in patients with myelodysplastic syndrome. *Anticancer Res* 1994; **14**: 2093–7.
27 Akahane T, Akahane M, Shah A, Connor CM, Thorgeirsson UP. TIMP-1 inhibits microvascular endothelial cell migration by MMP-dependent and MMP-independent mechanisms. *Exp Cell Res* 2004; **301**: 158–67.
28 Waltenberger J, Claesson-Welsh L, Siegbahn A, Shibuya M, Heldin CH. Different signal transduction properties of KDR and Flt1, two receptors for vascular endothelial growth factor. *J Biol Chem* 1994; **269**: 26 988–95.
29 Vega-Diaz B, Herron GS, Michel S. An autocrine loop mediates expression of vascular endothelial growth factor in human dermal microvascular endothelial cells. *J Invest Dermatol* 2001; **116**: 525–30.
30 Abe M, Sato Y. Puromycin insensitive leucyl-specific aminopeptidase (PILSAP) is required for the development of vascular as well as hematopoietic system in embryoid bodies. *Genes Cells* 2006; **11**: 719–29.
31 Endo H, Takenaga K, Kanno T, Satoh H, Mori S. Methionine aminopeptidase 2 is a new target for the metastasis-associated protein, S100A4. *J Biol Chem* 2002; **277**: 26 396–402.
32 Griffith EC, Su Z, Niwayama S, Ramsay CA, Chang YH, Liu JO. Molecular recognition of angiogenesis inhibitors fumagillin and ovalicin by methionine aminopeptidase 2. *Proc Natl Acad Sci USA* 1998; **95**: 15 183–8.
33 Yamazaki T, Akada T, Niizeki O, Suzuki T, Miyashita H, Sato Y. Puromycin-insensitive leucyl-specific aminopeptidase (PILSAP) binds and catalyzes PDK1, allowing VEGF-stimulated activation of S6K for endothelial cell proliferation and angiogenesis. *Blood* 2004; **104**: 2345–52.
34 Botbol V, Scornik OA. Measurement of muscle protein degradation in live mice by accumulation of bestatin-induced peptides. *Am J Physiol* 1997; **273**: E1149–57.
35 Inui K, Tomita Y, Katsura T, Okano T, Takano M, Hori R. H+ coupled active transport of bestatin via the dipeptide transport system in rabbit intestinal brush-border membranes. *J Pharmacol Exp Ther* 1992; **260**: 482–6.
36 Scornik OA, Botbol V. Cellular uptake of 3H-bestatin in tissues of mice after its intravenous injection. *Drug Metab Dispos* 1997; **25**: 798–804.
37 Ichinose Y, Genka K, Koike T *et al.* Randomized double-blind placebo-controlled trial of bestatin in patients with resected stage I squamous-cell lung carcinoma. *J Natl Cancer Inst* 2003; **95**: 605–10.

doi: 10.1111/j.1349-7006.2007.00393.x
© 2007 Japanese Cancer Association